

FUTURISTIC BEEHIVES FOR A SMART METROPOLIS

Deliverable D5.1

Design of the brood nest module

Lead Beneficiary	EPFL
Delivery date	31.03.2020
Dissemination Level	PU
Version	1.0
Project website	www.hiveopolis.eu



This project has received funding from the European Union's Horizon 2020 research and innovation programme under grant agreement No 824069

DELIVERABLE SUMMARY SHEET

Project number	824069
Project Acronym	HIVEOPOLIS
Title	FUTURISTIC BEEHIVES FOR A SMART METROPOLIS
Deliverable No	D5.1
Due Date	Project month M12
Delivery Date	31.03.2020
Name	Design of the brood nest module
Description	This deliverable describes the design of the brood nest module, which includes the design of the mechanical structure of the brood nest module with the integrated sensors, such as cameras and actuators.
Lead Beneficiary	EPFL
Partners contributed	UNIGRAZ, FUB, ULB
Dissemination Level	Public

Introduction	4
Purpose and scope of the document	4
Overview of the document	4
Acronyms and Abbreviations	4
Chapter 1: Objectives of the module, and survey	5
1.1 The importance of thermal environment in the brood nest	5
1.2 State of the art in brood nest thermal observation	6
1.3 State of the art in brood nest thermal manipulation	7
1.4 Goals of our system	7
Chapter 2: First prototype brood nest module	9
2.1 System design	9
2.1.1 General architecture overview	9
2.1.2 Sensory system	11
2.1.3 Thermal actuators	12
2.1.4 Imaging system	13
2.2 Experiments conducted	13
2.2.1 Observational experiments	13
2.2.2 Modulatory experiments	14
2.3 Results	14
2.3.1 Observations made using non-visual sensors	14
2.3.2 Analysis of brood images	17
Measuring colony activity	17
Background extraction	20
2.4 Observations and issues identified	21
Chapter 3: Second prototype brood nest module	23
3.1 Improving the design: building blocks	23
3.1.1 Selecting a temperature sensor	23
3.1.2 Selecting the density of temperature sensors	25
3.1.3 Selecting suitable sampling rates	25
3.1.4 Design for an integrated thermal actuator	26
3.2 The second brood nest module design	30
3.2.1 PCB design	31
3.2.2 Frame to house PCB	33
3.2.3 Full setup architecture	34
3.3 Discussion	36

Chapter 4: Integrated camera system for brood nest observation and mite infestation assessment	38
4.1 Importance of larval observation	38
4.2 Functional constraints	39
4.3 Implementation	40
4.3.1 Hardware design	40
4.3.2 Software	42
4.3.2 Development over time	42
4.4 Performed tests	44
4.5 First results	44
4.6 Conclusion on the camera module	48
4.6.1 General conclusion	48
4.6.2 Advantageous hardware settings and design paradigms identified	48
4.6.3 Suggested future tests / future questions to be answered:	50
Conclusion	52
List of Appendices	52
References	53

Introduction

Purpose and scope of the document

This deliverable presents the first designs of the brood nest module, which is a bio-hybrid system that interacts with the first life stage of the honeybee colony. The module comprises components for observation and modulation of the honeybees, and additionally for recording ground-truth data to correlate with the integrated sensors. The work contributing to the design here is made up of two distinct parts: interacting with the brood thermally (task 5.2) and developing an imaging system that is capable of capturing high resolution data (task 5.3) that will contribute towards quantifying the health state of individual larvae (task 5.4, not part of this report).

Overview of the document

The main body of this deliverable comprises four chapters. The first focuses on the global goals of the brood nest module, and situates the work in the literature context. The second chapter describes the first prototype sub-system for observing and modulating the honeybee brood nest thermally. This chapter details not only the design but also presents some of the data gathered during the summer of 2019. The third chapter describes our second prototype sub-system, which aims to address several issues that we learned about through the design, implementation, and experimentation with the initial prototype. The fourth chapter is dedicated to the individual larva observation sub-system development work, and describes exploration with various visual systems and analyses results acquired.

Acronyms and Abbreviations

Acronyms and Abbreviations	Definition
GPIO	General-purpose input/output
I2C	Inter-integrated circuit
MCU	Micro-controller unit
NAS	Network attached storage device
PCB	Printed circuit board
PWM	Pulse-width modulation
RH	Relative humidity
SBC	Single board computer
SPI	Serial peripheral interface

Chapter 1: Objectives of the module, and survey

The health of the larvae in the brood nest is paramount to the survival and growth of a honeybee colony. The overall objective of the brood nest module is to develop a bio-hybrid system that can observe the state of the brood nest, predict dynamics of future growth, identify health issues, and to support the colony through modulating key factors such as growth timing or location. We can identify the following goals:

1. identify the location and size of brood nest, as well as the health state;
2. Influence where and/or when the queen lays eggs;
3. Measure geometry of larvae, larval stage, visual properties over time.

Several requirements arise from these goals:

- Monitor the temperature distribution within the brood nest, at a spatial and temporal resolution sufficient to identify the regions with cells containing brood at a given point in time;
- Modulate the temperature in multiple areas within the brood nest module to influence egg-laying choices;
- Visual observation of larvae with certain image resolution and temporal resolution to measure geometric larvae parameters, as well as to detect parasites or other variations of the normal growth process.

In the chapters below we identify more detailed specification for the brood nest module that addresses the tradeoffs e.g. between information quality, cost, and energy consumption. The first part of this report concentrates on developing an embedded, non-visual, closed-loop sub-system which relates directly to task 5.2. The second part of the report concentrates on developing an imaging sub-system that aims to acquire detailed within-hive imagery of larvae and relates directly to task 5.3. Note that while both sub-systems involve visual acquisition components, the former uses only for validation purposes while the latter will be a part of the final HIVEOPOLIS units.

1.1 The importance of thermal environment in the brood nest

A honeybee colony tightly regulates the environment of its brood nest. The larvae are particularly sensitive to temperature during development (Tautz et al., 2003). Adult bees can increase the temperature by activating their flight muscles (Esch & Goller, 1991) and they enter empty cells next to occupied brood cells to transfer heat (Humphrey & Dykes, 2008; Kleinhenz, 2003). Workers can decrease the temperature by bringing in water to evaporate (Nicolson, 2009).

While 33-36 °C temperatures are maintained inside the brood nest, even with higher or far lower ambient temperatures outside the hive, other areas of the hive are not so tightly regulated (Dunham, 1931; Fahrenholz et al., 1989). Bonoan et al (2014) notes that even within the brood nest, different stages of development require different levels of thermal

regulation (see also Jones et al., 2005). This indicates a clear need for high-density thermal observation within the brood nest.

1.2 State of the art in brood nest thermal observation

In the trend towards increasing technology in agriculture (Meikle & Holst, 2015; Zacepins et al., 2015), the temperature is frequently one of the variables observed in beehives (Edwards Murphy et al., 2015; Ferrari et al., 2008; Howard et al., 2018; Mezquida & Martínez, 2009), sometimes in several locations throughout the hive (Giammarini et al., 2015 have 16 sensors around the walls of a hive; Meitalovs et al., 2009 have seven sensors -- one per wall, and one at the entrance), which brings value because there often exist important temperature gradients within the hive (Meikle & Holst, 2015). Researchers often position temperature sensors with respect to the colony, e.g. a sensor specifically in the brood areas (Gil-Lebrero et al., 2017) or in a standardised position with respect to the hive (Meikle et al., 2017).

The importance of temperature homeostasis in the brood nest has stimulated various works to observe the temperature dynamics and the behaviours responsible. Indeed, nearly a century ago Dunham (1931) monitored brood nest temperature dynamics, revealing small variation in the central brood nest, increased variation in the outer brood, and more so in broodless areas. Several studies have used infrared cameras, either to observe temperature distributions of brood nests (Bonoan et al., 2014) or profiles of individual bees (e.g., Bujok et al., 2002; Kleinhenz, 2003; Stabentheiner et al., 2010). Human et al (2006) placed temperature and humidity loggers in the brood nest and honey stores to investigate the homeostatic regulation effort of bees on temperature and humidity (one device in each area in each hive). Simone-Finstrom et al (2014) placed 8 probes across each of several brood nests to investigate the consequences of genetic diversity on the ability of a colony to thermoregulate the nest.

Fahrenholz et al (1989) used a special hive that had small plastic tubes inserted into the combs, and allowed moveable thermocouples to be placed inside to measure a specific point within the hive. The researchers moved the positions of the sensors according to where the brood nest or the winter cluster was located, without using a large number of sensors in total (they reported three locations: the centre of the bees; the periphery of the bees, and the hive entrance; but the number of sensors used is not stated).

Becher & Moritz (2009) developed a high density system comprising 256 NTC thermocouples, each positioned on the cell wall junction of three cells, thus monitoring 768 cells. This is the highest-density monitoring of a brood nest described in the literature. The device was mounted in a custom box with a regular honeycomb frame on one face, and the sensors attached to the back-side of the comb. It was tested in a hive with 3 standard frames and the special sensor/comb. The authors note that this organisation caused substantial differences in temperature on the front and back sides of the measured comb, and that usually the activity of workers on the back side of the comb would maintain a higher temperature.

Zhu et al (2019) developed panels comprising 36 digital temperature sensors, and inserted them either side of frames in a Langstroth hive, to monitor the temperature distribution

throughout the hive. Their aim was to predict swarming but the system itself could, in principle, be used to monitor brood nest temperature dynamics.

1.3 State of the art in brood nest thermal manipulation

Scientific investigations into the importance of temperature in honeybee brood nests have not been restricted to observational studies, but also considered actively changing the thermal environment to understand the effects and present mechanisms that aim to support a colony. For example, keeping hives in a heated building over-winter (Stalidzans et al., 2017; Zacepins et al., 2011) can significantly reduce honey consumption. Bayir & Albayrak (2016) developed a 36 W solar-powered inter-frame heater that was placed between standard frames, exploring thermal controller design (but did not report the impact on the bee colony). Altun (2012) developed a hive temperature regulating system using Peltier devices, which can both heat and cool using electric energy from solar panels. The study shows the heat functioning, but also does not report the impact on the bee colony. Other studies investigate specific temperature-related behaviours. In stingless bees (a tribe closely related to common honey bees) it has been shown that brood production can be increased during cold seasons by artificially heating a hive (Vollet-Neto et al., 2011). Bonoan et al (2014) used a strong thermal energy source outside of an observation hive that could reach only a part of the brood nest, and showed a “heat-shielding” behaviour in workers where they would attempt to absorb the external heat energy, and then moving away from the brood nest to transfer it away. Szopek et al (2013) investigated collective decision-making made by honeybee groups when presented with a choice of temperature hotspots, in a laboratory setting. Taking this further, collective choices can be made between honeybees and that adapt the temperature locally in response to the bees’ actions (Mills et al., 2015; Stefanec et al., 2017). Finally, some studies have placed adult bees or larvae in incubators to examine the responses in highly regulated conditions. Doull (1976) investigated the impact of humidity on larvae hatching rates, using incubators at constant temperature (35 °C) and constant humidity (20-100% RH). Kleinhenz et al. (2003) investigated the thermal production of individual nurses, comparing biological bees and “artificial bees” comprising small resistors placed inside bee thorax, and measuring how heat generated by each propagated into adjacent brood cells. Groh et al. (2004) incubated brood at temperatures between 28 °C and 38 °C and observed high emergence rates only between 31 °C and 36 °C, with 0% emergence at 28 °C and 38 °C.

1.4 Goals of our system

In terms of sensing the temperatures within the brood nest, the overall goal of detailed measurements is well supported by literature; however, the specific performance objectives (sensor precision, spatial density of sensors, sampling frequency) are not well established. Without strictly reaching performance requirements, we can identify some reference points to further evaluate from.

Regarding **sensing precision**, the literature reports various meaningful levels of precision for temperature in the brood nest: (Tautz et al., 2003) show that a difference of 1.5 °C affects development; Jones et al. (2005) shows 1 °C affects short-term memory; Stabentheiner et al.

(2010) uses a 0.2 °C threshold to denote whether an individual bee is heating a brood cell; and Bauer et al. (2018) shows that Varroa mites raise the temperature of larvae by 0.03-0.19 °C. Generally, we see a trend of increasing precision in reported measurements, and new phenomena are aided by improved instrumentation. We are therefore motivated to approach the tighter goals, while noting that any sub-degree precision will be informative.

Regarding **sensor density**, there exist thermal gradients within the brood nest as well as between brood and non-brood areas (Becher & Moritz, 2009; Humphrey & Dykes, 2008; Kronenberg & Heller, 1982). Detecting these thermal gradients should be informative for determining brood nest location and size. While in principle one could develop a per-cell measurement (see (Becher & Moritz, 2009) as described above), such resolution is too detailed and likely a poor allocation of resources for the objectives of estimating the brood nest location and size. Various studies consider temperature gradients surrounding a nest, but to our knowledge using temperature to estimate where brood exists on the frame (aiming to estimate which and how many regions, and thus also estimate brood quantity) is novel. Accordingly, later in this report we develop a model to assist with defining sensor quantities.

The rate of change of temperature in the brood nest should inform us regarding the **sensor sampling rate**. Measurements taken of a bee heating in the brood nest shown in (Kleinhenz, 2003) reveal a steepest change of approximately 2 °C in 10 minutes (0.1 °C / 30 sec) and similar rates appear in the modelling study of Humphrey & Dykes (2008). These measurements are both of individual heating bees rather than the temperature of larger patches with greater thermal inertia, and are likely rather extreme upper bounds. Sampling at or faster than one minute intervals should be feasible within our developed array.

Regarding modulation of temperature in the brood nest, we have less from the literature to guide us. Most of the artificial heating studies as described above either heat a whole hive (e.g. Stalidzans et al., 2017), heat a single patch (e.g. Bonoan et al., 2014), or are investigating the substitution of a single bee (Kleinhenz, 2003). The studies investigating collective decision-making (Szopek et al., 2013; Mills et al., 2015; Stefanec et al., 2017) begin to feature closed-loop dynamics that connect the bee behaviour and environmental modulation but were conducted outside of the hive environment.

Nonetheless, we can establish some key targets. The rate of change in temperature need not be greater than 2 °C in 10 minutes (Kleinhenz, 2003). The limits to upper temperature fall into two categories: a) long-term, where the heating actuators should not expose the brood to temperatures greater than 36 °C (Groh et al., 2004); and b) short-term capacity to emit higher levels of heat, e.g. 15 minutes at 46-48 °C as used in so-called “bee saunas” as part of treatment against parasites (Harbo, 2000). The controller design should keep overshooting phases to a minimum in either category. Towards the goal of influencing the egg-laying dynamics, the ability of young honeybees to collectively decide between thermal optima has been shown over spatial scales as large as 60 cm (Szopek et al., 2013) and as small as 9 cm (Stefanec et al., 2017), giving some indication regarding the actuator dimensioning. The breadth of possible experiments increases with the number of individually-controllable actuators; which implies an absolute minimum of two actuators to facilitate choice experiments. This capacity would also facilitate investigations into energetic support of raising brood.

Chapter 2: First prototype brood nest module

This chapter describes work towards the objectives relating to (1) brood location and size estimation, and (2) modulation of queen egg-laying, including an initial prototype system that gathered data during summer of 2019.

Given the short period during which honeybee brood develops and the start date of the project, one of the key constraints driving this prototype was timescale. The scientific objectives were: to determine whether we could identify the location of the brood with temperature sensors alone, and to ascertain the ability of thermal actuators to influence the behaviour of the queen, when in an open loop configuration.

2.1 System design

Our first prototype brood nest system comprises the following key elements: (1) an array of temperature sensors covering the brood nest frame, (2) heating elements inside the frame, and (3) a video system to obtain ground truth. The technologically enhanced frame was housed in an observation hive, alongside two conventional frames. This section describes the design of each of the parts of our system. Minute details of components, products, and software packages used are provided in Appendix B.

2.1.1 General architecture overview

General architecture: the brood nest frames with sensors and actuators were housed inside an indoor 3-frame observation hive with approximately 3000 bees (at peak conditions in August) (*Apis mellifera*) at University of Graz. Besides the custom brood frame, the system also includes CO₂ and humidity sensing, video cameras on each side of the frame operating under infra-red lighting. The system collected data from the hive continuously. Fig 2.1 shows the system and its components, and Fig 2.2 shows the system structure. The room where the hive was located has network connection and mains power. The hive orientation is oriented approximately East/West, i.e., the front comb faces East and the back comb faces West. Since it was indoors, the orientation is not particularly important for insolation but we define it here so to refer to particular faces or regions.

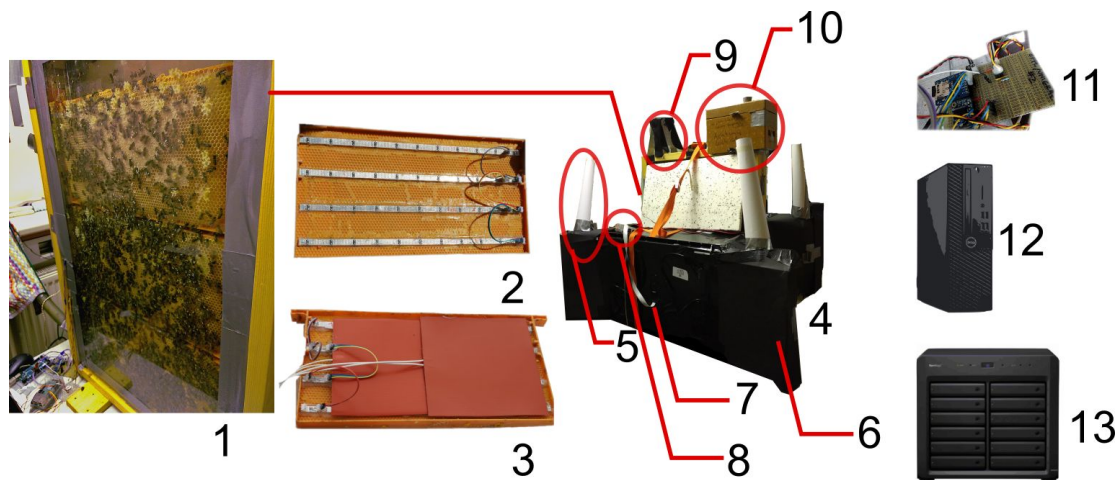


Fig 2.1: Overview of brood module, showing the system physical organisation and mechanical construction of the frames. 1) the open observation hive 2) inside view of a comb - strips with temperature sensors 3) heating elements on top of the sensor strips 4) the encased observation hive, styrofoam encasing for thermal isolation, black part isolate from outside light and house the camera and lighting system 5) as the infrared light produces some heat, paper funnels let the heat pass without letting ambient light in 6) infrared light (not visible here) 7) raspberry pi camera (V2 noir) 8) Raspberry Pi for image recording 9) bee feeder 10) box for bee interaction (e.g. varroa treatment) 11) Arduino based data logging board (for temperature data) 12) PC for storage of temperature data 13) NAS for image data storage

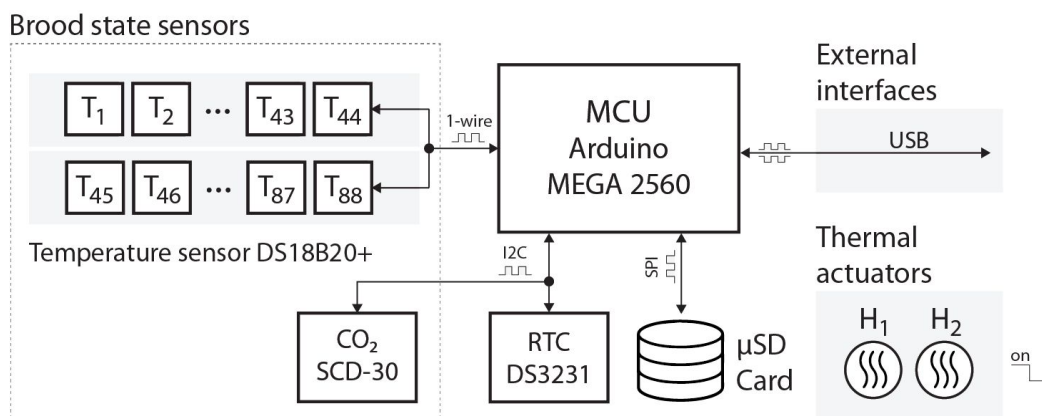


Fig 2.2: System block diagram for first brood nest module prototype, comprising a sensor array and open-loop thermal actuators. The temperature sensors are arranged in two banks, each bank monitoring one face of the brood nest. Data from all sensors is sampled periodically and stored locally as well as transmitted to a web-connected PC.

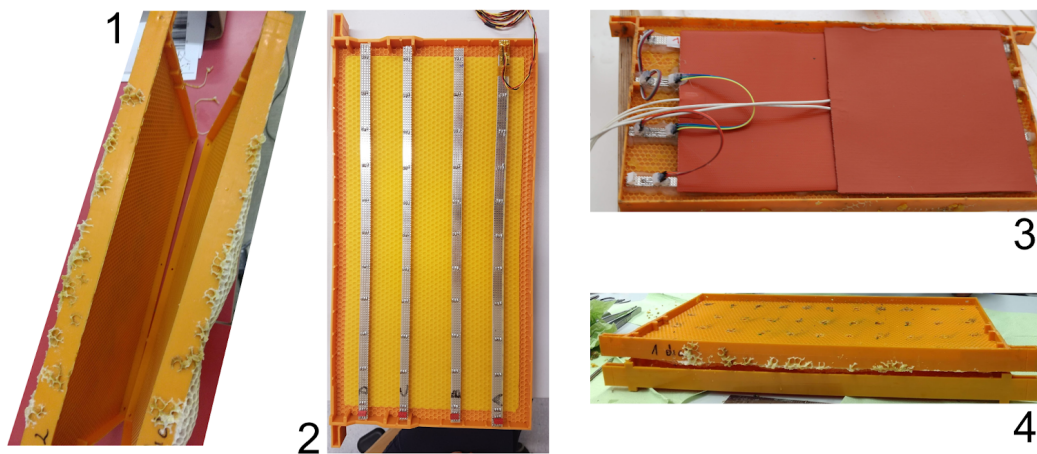


Fig 2.3: The double comb concept. 1) two ordinary plastic combs are put together to create a cavity inside a comb for sensors and actuators (before equipping them with sensors and actuators we placed the empty double-combs into the hives, so that they get accepted by the bees, wax comb is already fully built at this point) 2) the inside of each comb side gets equipped with sensor strips that contain temperature sensors that face outwards (inside view shown here) 3) temperature pads are placed on top of the sensors to modulate the temperature of the combs 4) both sides are put together again, the cavity between the two combs is filled with the sensors and actuators

Brood frame mechanical setup: Brood nest frames were constructed by connecting together two plastic foundations, leaving a cavity inside for sensors and actuators (see Fig 2.3). This construction had the advantage that they could be made before the season began, placed inside hives for bees to construct comb and establish brood, without the need for the electronic design to be finalised.

2.1.2 Sensory system

We had the objective to measure temperature at a fine spatial resolution and precision. For a prototype that could be assembled rapidly, we selected a popular and vastly offered Arduino Mega board, equipped with an ATmega 2560 8-bit microcontroller with a clock speed of 16 MHz, to work as an interface between the sensors, the real-time clock (RTC) and an external computer. The block diagram in Fig 2.2 depicts the logical connections in the system. All the collected data, sent through the USB - functioning as a virtual serial port - was also recorded in a microSD card to avoid loss of data in case of a disconnection between the external computer and the electronics inside the hive.

For the thermal sensing of the brood nest, we selected the Dallas DS18B20+ temperature sensor, in the TO-92 packaging format, which has an accuracy of 0.5 °C, a resolution of 1/16 (0.0625) °C. This sensor was also selected because of its low standby current, typically 3 µA at +125 °C, to avoid “thermal contamination” of the frame from self-heating. Each device has a unique factory assigned 64-bit address intended to allow the daisy-chain of multiple sensors in a 1-wire bus, facilitating the construction of a sensor grid able to cover a considerable portion of the frame (Zander frame; 420 mm x 220 mm, width excluding the tabs).

To determine the maximum number of sensors, constrained by the 1-wire bus capacitance limitations, we incrementally increased the number of sensors, reaching a maximum of 88 sensors. Surpassing that number of sensors, the total bus capacitance (from cabling, pins, connectors, etc.) was too big to allow the minimum rise/fall time for the 1-wire protocol signals (Awtrey, 2004). We split the 88 sensors in two arrays of 44 sensors (four strips of 11 sensors), for each face of the foundation comb.

Additionally, we selected a CO₂ sensor (Sensirion SCD-30) that also features a humidity sensor. The SCD-30 is capable of measuring CO₂ concentrations ranging from 0 to 10'000 ppm with an accuracy of $\pm(30 \text{ ppm} + 3\%)$ and repeatability of $\pm 10 \text{ ppm}$. The SCD-30 humidity sensor can measure in the range of 0-100 %RH with an accuracy of $\pm 3 \text{ %RH}$ (at 25 °C) and repeatability of $\pm 0.1 \text{ %RH}$.

The Arduino MEGA sampled the temperature array and the CO₂ + humidity sensor every 8 seconds ($\frac{1}{8} \text{ Hz}$), stored the time-stamped data to the attached SD card and transmitted via a serial connection to a PC which periodically synchronized with a web-server, enabling remote access to data.

2.1.3 Thermal actuators

Thermal Actuators: Four heaters with target power generation of $\sim 3 \text{ W}$ each were built into the interior of the comb. Each side of the comb was equipped with two thermal actuator elements with a size of 190 x 190 mm, shown in Fig 2.4. Each heating element is a custom produced etched foil element, encased between two layers of silicone rubber, designed for a max. power consumption of 20 W. In our system each element is driven by a 5 V power supply and generates 3 W when activated. To activate the actuators we manually configured the connections. Although any combination of the four was possible in principle, we only used three combinations: all off; front-left + back-right; and front-right + back-left, defined when looking at each comb. Thus, either the North half of the combs were heated, or the South half (never crossed).

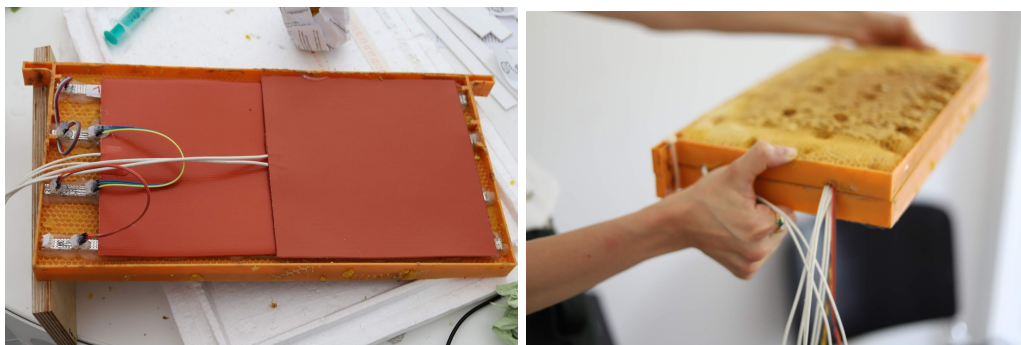


Fig 2.4: Thermal actuator elements, each comb side is equipped with two heating elements. The double-sided comb contains four heating elements, two of which are turned on and driven with a constant energy input of 3W each.

2.1.4 Imaging system

We observed the brood nest frames with cameras to obtain ground truth data regarding the cell usage in the frame, including capped brood cells.

Each of the two top-frames is observed by a dedicated Raspberry Pi (RPI) equipped with a Pi NoIR Camera V2. The brood frames are each continuously lit by two IR lamps (12 W each, wavelength: 840 nm) at each comb side placed left and right of the comb at a distance of approx. 30 cm. The lamps are angled in such a way that reflections from the light at the glass of the observation hives were minimized as much as possible. Each RPI executes two scripts: the first to set up and run the camera; and the second to regularly upload the photos to a network attached storage device (NAS). The camera first adapts to the lighting conditions for 4 seconds, after which the camera settings are fixed, such that all successive photos are taken with the same settings. Photos are taken every 4 seconds at a resolution of 1920 x 1080 (width and height, respectively) and stored in JPG format. Each day, the cameras each take 21,600 images of the brood frame, and these are periodically transferred to the NAS by the second script. This corresponds to approximately 30 GB of data per day.

To ensure reliability, systemd ensures the camera script is started after boot (and restarted in case of a crash). This method has been reliably running since the middle of December 2019 (with a coverage of >99% image collection rate). For the period from July to November 2019, a less robust system was implemented on the RPi computers that was less reliable and resulted in some gaps in the data. Nonetheless we obtained ~2.5 million photos (a ~45% coverage of that timespan) allowing for some preliminary analyses (see section 2.3).

2.2 Experiments conducted

2.2.1 Observational experiments

The initial system (double comb equipped with temperature sensors) was set up during the HIVEOPOLIS workshop in Graz between 11.06.2019 and 14.06.2019. Cameras and lighting were added to the hive afterwards, and around the beginning of July we started to acquire image data in addition to the temperature data.

Besides validating the designed functionality, we also aimed to assess whether the selected design and components were adequate. Several indicators for the general health state of a bee colony can be ascertained through observations on the brood nest. These include the number, the duration and the strength of the form of the breeding cycles over the summer, the general activity of the bees on the brood nest, the difference in the activity of the summer bees and the winter bees depending on the ambient temperature and the temperature of the brood comb. All of these indicators can be derived from the cell content configuration on the brood comb, therefore we had to find ways of observing changes on the comb itself without the bees moving on the comb and thus disturbing our observations. To test various methods of background calculation we needed a sufficient dataset. To date, the system continues to record data (21.03.2020).

2.2.2 Modulatory experiments

On 04.07.2019, the system was expanded to include an active component. In order to investigate the effect of external temperature sources onto the bee behaviour, the system was equipped with four heating elements. At the beginning of the winter period (06.09.2019), two of these heating elements were activated, so that one half of each comb was heated. The impact of a very low energy input should be examined: 3W of energy was supplied to an area of 361cm² of constant heat on each side of the honeycomb (about half of the comb, 8.31mW / cm²). In our initial experiment, the bees reacted to this additional energy and formed the winter cluster at the area of heat supply. In addition, the heat supply side was switched towards the end of the winter season (06.03.2020) to observe whether the bees would react to a change of the energy input at a later time.

2.3 Results

We started to collect sensory data from June 2019, and after revising the hardware in late July 2019 we now have a more reliable dataset. The ground-truth image acquisition was commissioned a short while afterwards and continuous data collection started in late July. Both components suffered some data losses (described below) but this should not overshadow the data that was collected and the trends that our initial analyses are able to reveal.

2.3.1 Observations made using non-visual sensors

The SCD-30 combined CO₂, temperature, and humidity sensor was located above the top comb in the observation hive and captured some of the internal environment. Fig 2.5 shows the time-course of these three variables over the course of two months, which reveal clear daily cyclic values in temperature and humidity but less so in CO₂. Note that the CO₂ levels are extremely high in comparison to the open environment (in the range 405-415ppm for 2019) but not inconsistent with some other reports in the literature (e.g., Ohashi et al., 2009). In September the CO₂ and temperature exhibited a sharp increase which seem to be a form of colony response to the thermal actuators being switched on, but interestingly the high levels were not maintained despite the actuators being active until beyond the end of the period shown here.

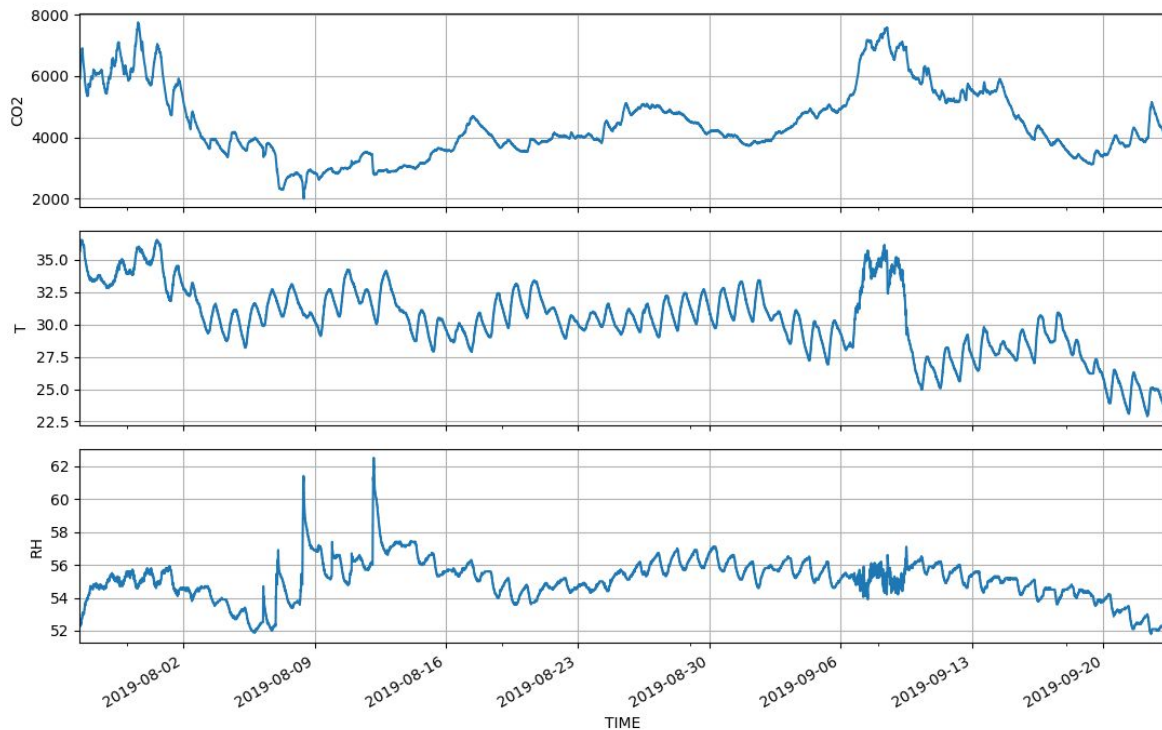


Fig 2.5: Time course of CO₂, temperature and relative humidity, recorded inside the observation hive over two months. Note the daily cycles within temperature and RH but not in CO₂ trends.

From the temperature array the quantity of data produced is not trivial to visualise in a way that is both informative and quick to reflect on. The presentation in Figs 2.6 and 2.7 shows the time course of temperature for each day on each sensor, in the spatial layout of the sensor array. These two figures show the progression within weeks 31 and 34 of 2019. Fig 2.6 is indicative of two basic classes of temperature profile. In the centre of the image, there is a low variance in temperature through each day, while towards the periphery the temperature climbs through the day and falls through the night and early morning. In Fig 2.7, just a few weeks later, almost the entire array reveals the cyclic trends.

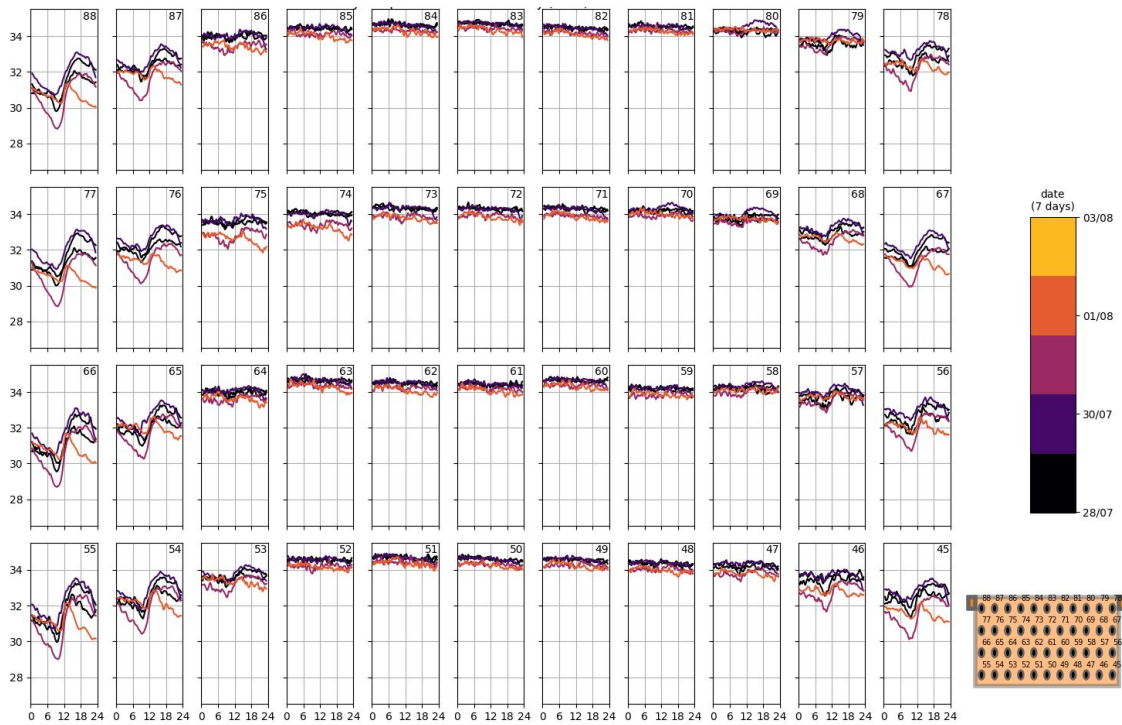


Fig 2.6: Daily temperature trends, for five days starting 29.07.2019 (colour shows progression in days, each subplot x-axis spans midnight to midnight). This mesh of subplots show a clear spatial pattern and can be categorised into two basic classes: tightly regulated, and cyclic. Fig 2.8 visually shows where capped brood cells are located at one snapshot during this week, and the correlation between fraction of brood cell and regulation tightness is intriguing. Statistically robust predictors remain to be identified.

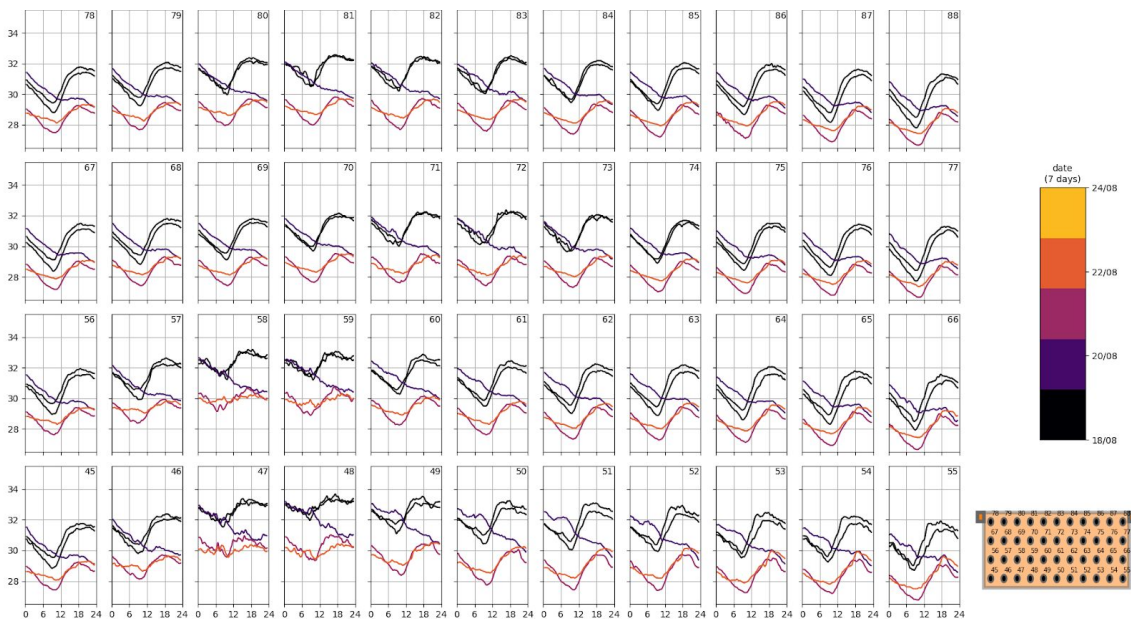


Fig 2.7: Daily temperature trends, for five days starting 19.08.2019 (colour shows progression in days, each subplot x-axis spans midnight to midnight). Here, the manual inspection revealed less than 5% capped brood. Nearly the whole mesh appears to follow environmental temperature trends; unlike the bi-modal signatures observed in Fig 2.6.

The thermal profile above (Fig 2.6) is incomplete without a ground-truth annotation of what state the brood nest is in. Here we provide a first glimpse into the relationship between the brood state and the information available from the temperature sensor array (Fig 2.8). This makes use of bee-free images obtained with the background extraction technique (described below, in Sec 2.3.2), and manually annotated the cell usage.

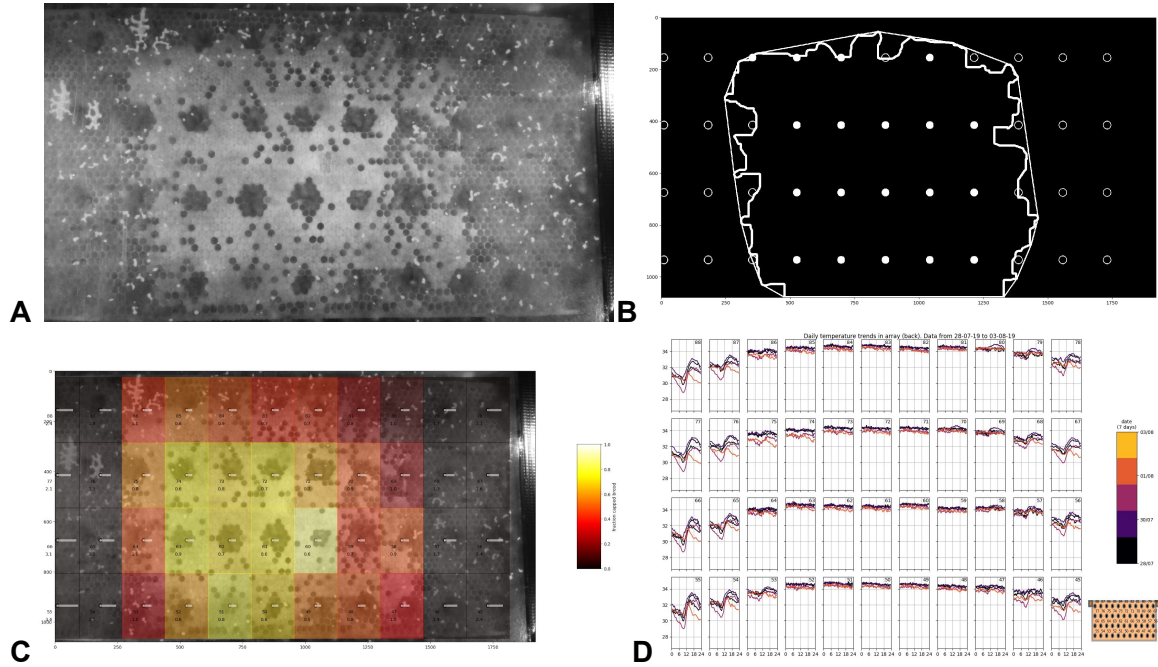


Fig 2.8: Brood nest annotation. A) Brood nest with “bee removal” applied. B) After hand annotation of capped brood cells, extraction of perimeter. C) heat map showing fraction of capped brood cells per grid cell belonging to each temperature sensor. D) daily trend of temperature for each sensor (colour shows trend on different days).

2.3.2 Analysis of brood images

For all primary image analysis purposes detailed in this section, OpenCV 3.4 was used (with Python 3.6+).

Measuring colony activity

To provide a coarse measure to assess the general activity of the observed bees, we compute the Manhattan distances between consecutive photos (the sum of the absolute differences between all pixels) without any additional image processing. Since the photos are recorded exclusively in IR-light, the differences between the three RGB channels of the image are negligible and we can treat each as a single layer greyscale intensity array. With $I_{i,j,t}$ the intensity of a pixel (i, j) , the Manhattan distance D_M between two images (from times $t-1$ and t) is given by:

$$D_M = \sum_{i=1}^{1080} \left(\sum_{j=1}^{1920} |I_{i,j,t} - I_{i,j,t-1}| \right)$$

This metric is very noisy for any given 4 second interval -- and extremely susceptible to ever so small changes in relative camera-position -- but by averaging the data into hourly bins (using the median), these problems are circumvented. A circadian pattern is clearly visible in the recordings, with activity peaks corresponding to noon (in fact to approximately 2 pm local time) and lulls to night time (see Fig 2.9). Mapping the hourly medians from 28.07.2019 to 11.08.2019 (as shown in Fig 2.9) to a single day (and assuming independence between the days), functional boxplotting can be used to show that most diurnal activity curves follow a similar pattern (Fig 2.10). These daily activity trends are consistent with other observations in the literature. For instance, Southwick & Moritz (1987) observed significantly higher fanning behaviour during the day than during the night, and Klein et al (2014) found that forager activity cycles are strongly diurnal, active during the day and sleeping at night and with peak thorax temperatures from 12:00-18:00; patterns not observed in other castes. In the longer term, we see greater variation in diurnal activities and seasonal trends are to be expected, at least to the extent that activity in the brood frame is related to foraging activity (see, e.g., Lecocq et al., 2015 who observed seasonal variation in foraging through weight changes in hives). The patterns detected with this method are primarily due to the motion of bees on the brood frame: the alteration of the individual cell-surfaces (e.g., by capping) plays out on larger timescales and is a comparably rare event.

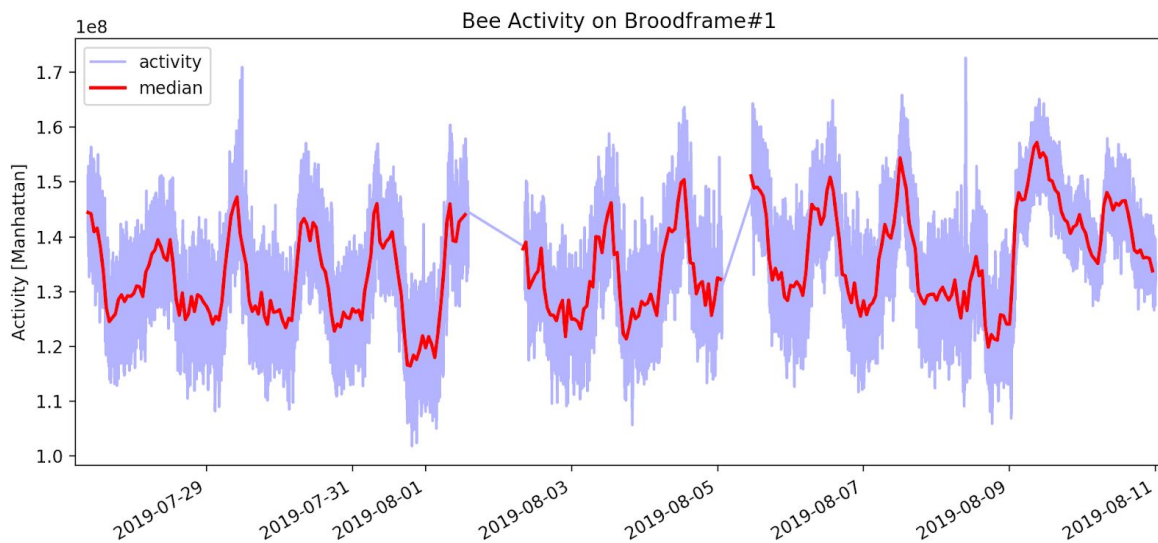


Fig 2.9: Manhattan distance between consecutive photos of brood frame#1 for the 14 day period from 28.07.2019 to 11.08.2019. In light blue, all measurements are shown; the thicker red line shows the hourly medians. Larger chunks of data are missing on 01.08, 02.08 and 05.08.2019 (indicated by a straight blue line without medians). Extreme outliers (due mostly to camera position changes) have been excluded.

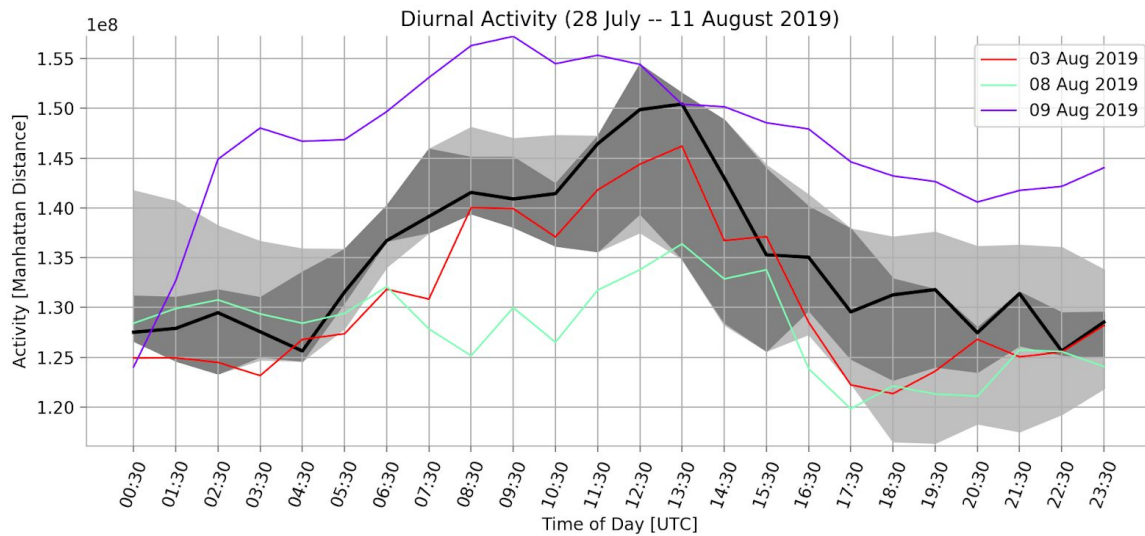


Fig 2.10: Functional boxplot¹ (with weight factor = 20) of the hourly medians shown in Fig 2.9, but mapped to a single day. The thick black line is the “median daily activity curve”; the dark grey area surrounding it can be interpreted analogous to the boxes in normal boxplots, the light grey area to the whiskers. The colored lines are “outlier-functions” (any curve that is an outlier at even a single hour, is considered such as a whole). For functional boxplotting, all the provided curves must have the same length, thus only days for which complete data was available could be used here (01.08, 02.08 and 05.08.2019 have been excluded). The peak in the median curve occurring around 13:00 UTC corresponds to 14:00 in local time (CET).

On the dataset from July to November 2019, a comparison with the (computationally more intensive) Euclidean distance revealed that the Manhattan distance qualitatively shows the same circadian pattern, with comparable relative scaling between maxima and minima. In fact, the extremes are slightly emphasized with Manhattan distance, making it the method of choice (being both faster and “better”). More involved methods for activity measurement of bees on the brood frame – with additional cropping and binary thresholding – are under development for other purposes within the project but have not yet been applied to the dataset in question here.

A glimpse at the colony activity over almost eight months is shown in Fig 2.11. This figure is far from perfect, owing to the restrictions imposed to counter the spread of COVID19 in Austria: We currently cannot physically access the network drive, where the photos are continuously being uploaded to. To keep infrastructure use modest, we sampled the data and downloaded only two hours worth of photos every day (and only from brood frame#1), resulting in ~250 GB of the ~6GB dataset. We downloaded all photos from 02:00–03:00 and 14:00–15:00 CET. The latter timespan roughly corresponds to the activity peak as detected in summer, while the former one is the night-time hour giving equal spacing (11 hours) between the samples.

¹ <https://www.statsmodels.org/stable/generated/statsmodels.graphics.functional.fboxplot.html>

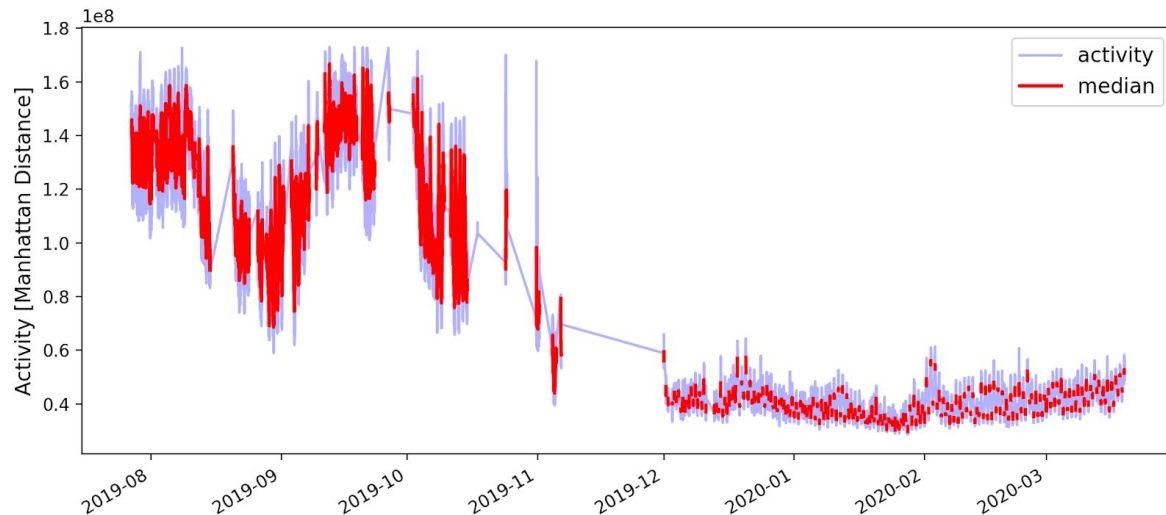


Fig 2.11: Long-term data of activity on brood frame#1 from 27.07.2019 to 20.03.2020. The vertical axis shows the Manhattan distance between two consecutive images (as in Fig 2.9). For the period July-November 2019, data from the whole day is treated; while from December 2019 to March 2020 two one-hour samples are analysed per day. See main text for details.

In the data shown here, there is an absolute minimum of colony activity in the last week of January 2020, after which activity steadily increases again. This trend is more pronounced when looking exclusively at either just the noon- or the night-samples (data not shown). Regarding the comparison between the data recorded in summer and winter, it has to be cautioned that the method for recording the images has changed in early December (with analog and digital gains as well as other camera settings fixed between shots), which could have contributed to a generally lower detected activity in the winter months. Yet, the data clearly shows diurnal activity changes and is indicative of seasonal trends to be looked out for in the coming season(s).

Background extraction

To observe the dynamics of the brood nest, it is imperative to get a possibly clear view of the individual cells of the waxcomb. To this end, batches of 200-400 images, corresponding to ~15-30 minutes in real time, were pooled to extract single background images, i.e. to visually clear the image of the bees moving over the cells. We tested 46 background subtraction methods from the OpenCV library, and selected among them based on their processing output (subjective/visual assessment) and how long each one took. We settled on the OpenCV *BackgroundSubtractorMOG2* algorithm.

This method was used to extract backgrounds four times a day (at 00:00, 06:00, 12:00 and 18:00 local time (CET)). During times of higher colony activity (see above), background extraction naturally worked better (i.e., when bees don't move much, they are considered "background" by the algorithm). Fig 2.12 exemplifies the background extraction process. The objective here is to monitor breeding dynamics of the colony and have early-warning systems in place for problems thereof and/or sudden deviations.

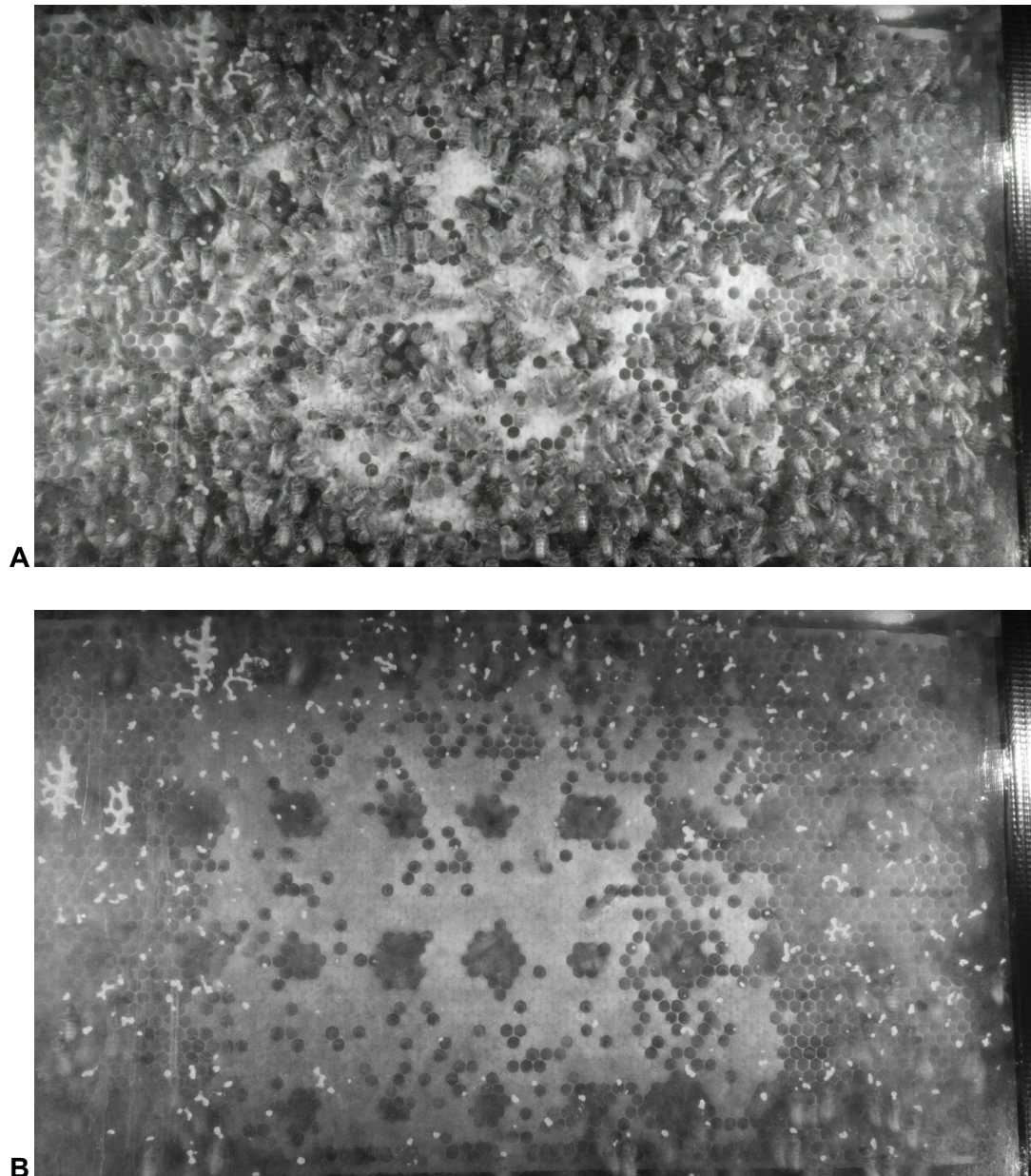


Fig 2.12: A) Photo of brood frame #1 on 28.07.2019 at 14:00:01 UTC. B) Extracted background from 200 photos (from 13:46:44 to 14:00:01). Capped and uncapped cells are clearly visible. The regularly spaced regions of uncapped cells indicate the positions of the temperature sensors (behind the wax), that seem to irritate the bees.

2.4 Observations and issues identified

The brood nest observation system assembled for experimentation during summer 2019 yielded interesting patterns regarding the bee colony and valuable information regarding what works and areas for improvement. The most critical issues can be split into two sub-groups, relating to: (1) the electronic sensory system; (2) the mechanical setup.

The electronic system became damaged after some weeks of exposure to the hive, and sensor data acquisition stopped. We suspect that the failure was due to additional capacitance on the sensor bus which arose from materials of the bee colony. Due to the single, in-series sensor design we lost access to all sensors. After diagnosing and rebuilding the system with better sealant around the sensors (using silicone), the revised construction was more robust and collected data for over six months. The measurement was operational, but the revised construction caused a biocompatibility issue: the bees seemed to be frustrated by each of the sensors, and no brood was raised within a radius of 1-2 cells of the sensor. Although self-heating of the sensor is unlikely a detectable issue (the average current draw is $<95 \mu\text{A}$ at the 8-second sampling interval), the physical size of the sensor, at $5.2 \times 4.2 \times 5.3 \text{ mm}$, could have been the problem.

In the mechanical setup we identified two issues. The double-comb construction left an air gap that had non-trivial thermal insulation, and this seemed to decouple the bees' activity on each side of the comb. This deviates somewhat from a typical situation where the brood nest on each face typically overlaps significantly: for example, Kronenberg & Heller (1982) reported a mean of 80% with a range of 49-97% overlap between two faces of the comb. Since the warmth generated by workers heating on one side will be conducted to the other side of the comb (see e.g., Humphrey & Dykes, 2008), it takes less effort to raise brood in the same location on the reverse side. Moreover, Becher & Moritz (2009) reported a temperature difference of approximately 1.4°C between front and back in their device, which also used a construction that prevented the bees' access to the reverse side of the comb. The second issue noted is more minor: the camera position with respect to the brood frame was not perfectly constant throughout the measurement period. Since we did not have registration marks on the frame either, the movement in image perspective made the analysis slightly more difficult.

From these observations, we identify several areas for improvement within the design of the second iteration, as described in Chapter 3. Regarding biocompatibility, we will (1) select smaller sensors that are less intrusive, and reduce the power consumption, (2) better isolate the electronic circuitry from the bees using a conformal coating, (3) develop a PCB with sensors and thin heating elements, will remove the insulating effect of the air-cavity in the double-frame design. Regarding the camera system, we will (4) include an IR LED on the underlying PCB, which can be used to demark location and confirm synchronisation between camera and embedded sensory systems, (5) construct a rigid scaffolding to ensure the positions of the cameras is stabilised, (6) use the improved version of the single-board computer code for image acquisition as described in Sec 2.1.4.

Chapter 3: Second prototype brood nest module

This chapter describes the second iteration of our brood nest module design. The design is significantly improved in comparison to the first prototype, and takes into account issues encountered and limitations identified through experiments with the first prototype. These issues are outlined at the end of the previous chapter. The goal of the second prototype is to facilitate the same two scientific objectives: to identify the location and size of the brood nest solely through temperature data; and to influence the behaviour of the queen through thermal actuators. Details of specific components, products, and software packages used are provided in Appendix B.

3.1 Improving the design: building blocks

3.1.1 Selecting a temperature sensor

Based on the knowledge acquired in the first system iteration, we surveyed integrated temperature sensors to select the best suitable candidate for the new system. We used the following requirements as selection parameters:

1. A small sized sensor (smaller than previously used package, TO-92) to minimize the impact caused by its presence on bees behavior and capable of being fitted inside a cell (typically a hexagon with width ≥ 4.5 mm);
2. Low power consumption to minimize self-heating of the sensor;
3. Minimum specifications (e.g., accuracy, resolution and precision) following values found in the literature, and in the first prototype iteration, to measure the biological events of interest.

Table 3.1 summarizes the technical specifications of selected temperature sensors.

Table 3.1 - Specifications of the temperature sensor candidates

model	op. range		res. (°C)	accu. 20-45 (°C)	supply		I_{SBY} (μA)	dimensions		
	min	max			range (V)	I_q (μA)		w	l	h
	(°C)							(mm)		
TE TSYS01	-40	125	0.01 (1/100)	0.1	3.2–3.4	12.5	0.14	4	4	0.85
TI TMP117	-55	150	0.0078 (1/128)	0.1	1.8–5.5	3.5	0.15	2	2	0.8
TI TMP175	-40	125	0.0625 (1/16)	2	2.7–5.5	85	3	3	3	1.1
Silabs SI7051	-40	125	0.01 (1/100)	0.13	1.9–3.6	120	0.62	3	3	0.75
Dallas DS18B20+	-55	125	0.0625 (1/16)	0.5	3.0–5.5	1500	1	3	3	1.1
Dallas DS28EA00	-40	85	0.0625 (1/16)	0.5	3.0–5.5	1500	1.5	3	3	1.1
Maxim MAX30205	0	50	0.0039 (1/256)	0.3	2.7–3.3	600	3.5	3	3	0.75
Maxim MAX31725	-55	150	0.0039 (1/256)	0.5	2.5–3.7	800	3.5	3	3	0.75
Sensirion STS30	-40	125	0.01 (1/100)	0.2	2.15–5.5	1500	2	2.5	2.5	0.9
Sensirion STS35	-40	125	0.01 (1/100)	0.1	2.15–5.5	1500	2	2.5	2.5	0.9
ADI ADT7420	-40	150	0.0078 (1/128)	0.2	2.7–5.5	300	15	4	4	0.75
Microchip MCP9808	-40	125	0.0625 (1/16)	0.25	2.7–5.5	200	0.1	2	3	1.1

The part survey led to the identification of two last-round sensors for further evaluation: MAX30205 (Maxim) and TMP117 (Texas Instruments). The MAX30205 part is 30% cheaper and supports 32 unique addresses (cf 4 addresses with TMP117). However, the operating range of 0 to 50 °C was considered too narrow².

We therefore decided to use the TMP117 sensor which has a broader temperature operating range (-55–150 °C), when compared to the MAX30205, a resolution of 1/128 (0.0078) °C, and package size (2 x 2 x 0.8 mm) capable of being embedded into a honeycomb cell. Moreover, the device, when in sampling mode, has a current consumption of 3.5 µA, and when in standby mode of 0.15 µA³. It offers four unique addresses, and we expand the quantity connectable to one I2C channel using 8-channel multiplexers.

We prepared a small evaluation board to examine the two last-round sensors, with three TMP117 and three MAX30205 devices (Fig 3.1). We used it to verify the sensor operation was suitable, and the placement was feasible at one sensor per cell spacing. Data only shown for the TMP117 sensors. The maximum difference between readings was 0.1°C which is within the datasheet tolerances, and the changes in temperature are highly correlated between all three sensor pairs.

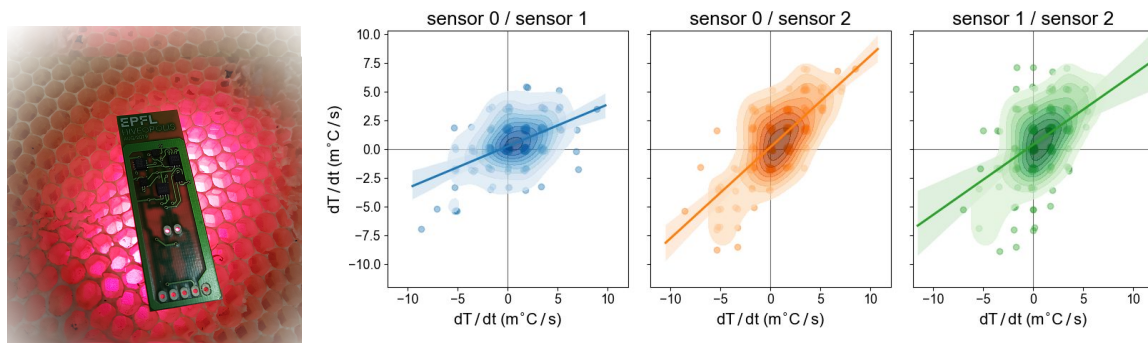


Fig 3.1: A) Temperature sensor evaluation board with three sensors of each type, shown on natural honeycomb for size reference. B) Data reliability between multiple TMP117 sensors - the change in temperature between subsequent samples is strongly positively correlated.

² Devices that routinely approach their limits can suffer accelerated fatigue or become damaged; Bujok et al. (2002) measured thorax temperatures at up to 42.4 °C for bees heating brood cells, while temperatures in unoccupied regions of a hive can drop to a few degrees above ambient, e.g. Owens (1971) reported -10 °C inside a hive on a day with -14 °C.

³A simple self-heating assessment can be made using the thermal resistance of each temperature sensor when in the most power demanding mode (i.e.: maximum dissipation). The change in temperature, between the IC junction and the ambient, can be estimated through the following expression: $\Delta T [^{\circ}\text{C}] = \Theta_{JA} [^{\circ}\text{C}/\text{W}] \cdot P_D [\text{W}]$. For the first prototype sensor, DS18B20, we estimate a maximum temperature rise of $\sim 1.5^{\circ}\text{C}$ when operating continuously ($P_D \sim 9.85 \text{ mW}$ and $\Theta_{JA} = 160^{\circ}\text{C}/\text{W}$ for a TO-92 package, see (Linear Technology, 2020)). For the TMP117 we calculated a maximum rise of $\sim 0.16^{\circ}\text{C}$, also assuming a worst case scenario of 100% duty cycle ($P_D \sim 2.3 \text{ mW}$ and $\Theta_{JA} = 70.7^{\circ}\text{C}/\text{W}$).

3.1.2 Selecting the density of temperature sensors

Our instrument will remain in place throughout the season, and we thus anticipate brood to be laid in several different areas on each brood frame over the course of each season. Therefore, we wish to measure temperature across the entirety of the frame.

In the first prototype, we selected the number of sensors based on an engineering limit (the channel capacitance). Clearly the more sensors used the greater the spatial resolution measurable, but there are diminishing returns for the financial, energetic, and design costs.

Here we approach the density selection through a simulation model which helps us to quantify the expected measurement error. The model and analysis is detailed in Appendix A, and took into account geometric constraints of the cell structure and frame dimensions, and the trade-off between sensor quantity (and therefore engineering effort, price per board, etc) and measurement quantity. Using this analysis we identified an array of 5 rows by 11 columns of temperature sensors. The final layout of the sensors is shown in Fig 3.2.

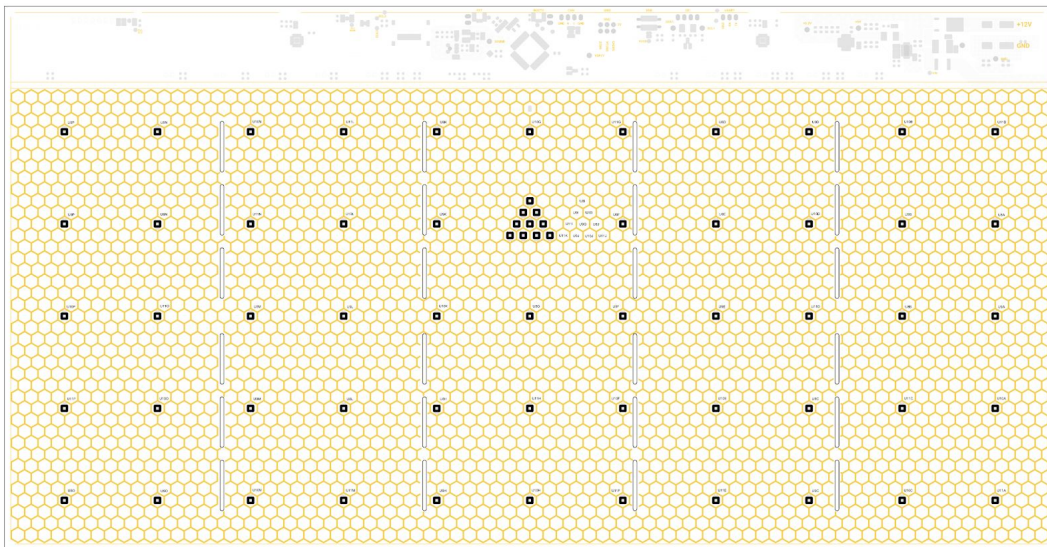


Fig 3.2: Illustration of brood nest PCB, with 55 sensors in 5 rows of 11. Given the relatively straightforward addressing of up to 64 sensors, we also included 9 extra sensors in an upper central position, at a density of one per cell, to investigate fine-scale temperature gradients. Other components faintly shown are detailed in later sections.

3.1.3 Selecting suitable sampling rates

An uninformed, cautious scientist records the highest rate technically possible, and the reasons for very low sampling rates would come from minimising required human effort or battery consumption in an autonomous system. Since our selected sensor can sample at >50Hz, and thermal dynamics are rather slow within a beehive, it makes no sense to generate uninformative high-frequency data.

We approach this issue by inspecting data from our 2019 system, which sampled temperatures on an 8-second interval.

From a sample of 7 days of temperature array data (October 2019), approximately 82% of the consecutive samples do not differ at all on an 8-sec sampling interval. This figure only drops to 73% on a 120-sec sampling interval. Figure 3.3 shows the mean absolute error when subsampling data points, interpolating the values at the intermediate points (where true values are known), and then computing the difference. With a sampling interval of 10 minutes, the greatest mean absolute error across all 44 sensors in the array still does not exceed the resolution of data reported by the DS18B20 sensor.

Note however that the data from temperature sensors in the first prototype might never have experienced the fastest rates of temperature change, i.e., those generated by brood-heating bees (Kleinhenz, 2003; Bujok et al., 2002). This is due to the rejection by the bees of the cells close to the sensor (see Sec 2.4), meaning that the faster dynamics may not have been sensed. Accordingly, we will start with cautiously high frequency sampling and reapply a similar analysis on data gathered with the second prototype hardware.

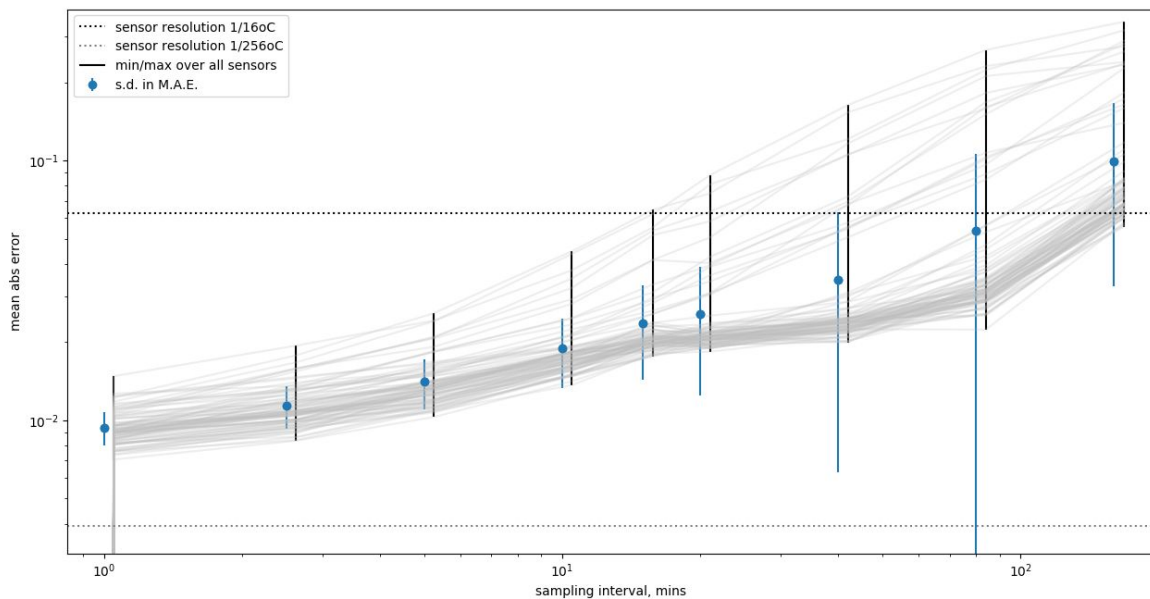


Fig 3.3: Results of sampling rate analysis achieved through sub-sampling the data at various extended interval times.

3.1.4 Design for an integrated thermal actuator

In this section we describe our design of a thermal actuator that is built into the same PCB that hosts the temperature sensors and forms the backbone of the comb foundation. The overall objective is to facilitate experiments into modulating the honeybee colony behaviour in the brood nest, specifically with respect to the location and timing of where eggs are laid and brood is raised. In Chapter 1 (see Sec 1.4) we identified some guidelines for

functionality. In brief, we aim for multiple thermal actuators that are individually controllable and possible to switch on specific groups of actuators simultaneously; that can maintain temperatures in the region 32-36 °C; and the control operation should have modes that strictly do not exceed 36 °C, while a special mode with higher heat emission for short periods could also be of interest. Due to the sensitivity of honeybees to temperature gradients, a homogenous emission of heat from an active element is important. The quantity of actuators should be selected based on the trade-off of controllability and costs; greater numbers could facilitate investigation with more diverse spatial patterns, but this prototype aims to prove concepts for the rather novel application - we fully anticipate further iterations in design to incorporate new knowledge.

Current flowing through a resistor will dissipate some energy in the form of heat – Joule heating (electrical energy → thermal energy). Following this principle we can design a conductor, with a specific value of resistance, that will dissipate power in the form of heat when connected to an electrical power supply ($P_{\text{heat}} \sim I^2 R$). Brooks & Johannes (2015) developed a model for the temperature change of an external trace for varying intensities of current. This model has similar results as the IPC-2152 standard⁴, which defines these values empirically. The model has the following form:

$$\Delta T [^{\circ}\text{C}] = 215.3 \cdot I^{2.0} \cdot w^{-1.15} \cdot th^{-1.0}$$

Where I is the current in Amps, w , the trace width in mils and th , the conductor thickness (or height) in mils. Fig 3.4 displays the result of the previously mentioned model, for five different conductor widths (5 to 50 mil) and copper weight of 1 oz (~0.035 mm).

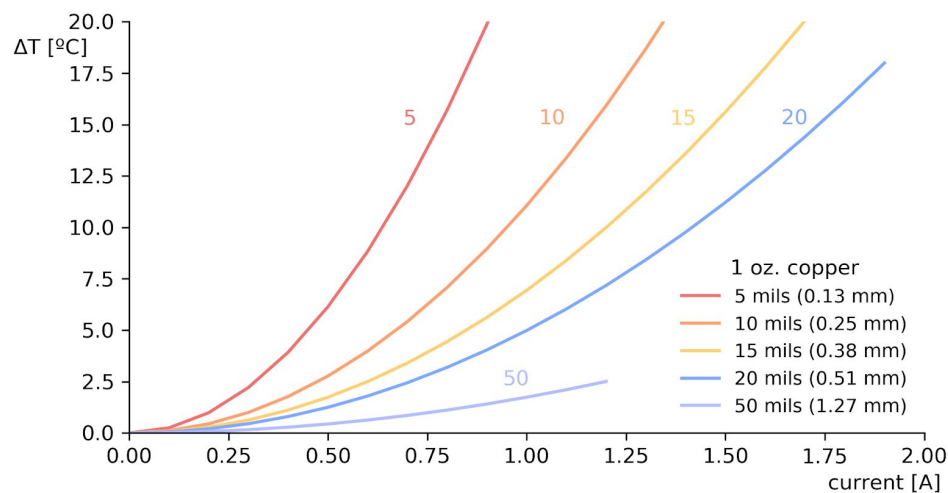


Fig 3.4: Temperature change as a function of input current.

⁴ IPC-2152, “Standard for Determining Current Carrying Capacity in Printed Board Design”

We wanted a trace size where not too much current was necessary to increase the temperature ($\Delta T_{\max} < 15\text{ }^{\circ}\text{C}$) but also not with a very low resistance so a small change in current flow would cause a big change in temperature. We decided to use a trace width of 0.267 mm (10.512 mils) and copper weight of 1 oz., which is expected to have a behaviour close to the orange curve from Fig 3.4. Based on an IPC-2152 calculator (Saturn PCB Toolkit v7.08), that trace is able to withstand a maximum continuous current of 1.85 A.

This model indicates that the maximum necessary current to change the temperature by 15 $^{\circ}\text{C}$ should be 1.195 A. Using Ohm's law, $V=RI$, and selecting a voltage source of +12 V_{DC} , a resistor of $\sim 10\text{ }\Omega$ would be required to create the necessary current flow. For practical reasons, we selected a resistance of 9.1 Ω . This slightly lower value allows for a margin to increase the heating power. Moreover, there are readily available COTS (E24 series) resistors of this value which facilitates simpler testing of the driving circuit.

The resistance of the planar heater can be calculated through the expression $R = (\rho \cdot L)/A$ [Ω], here ρ is the resistivity of the copper ($\sim 1.72 \times 10^{-8}\text{ }\Omega\cdot\text{m}$ at 20 $^{\circ}\text{C}$), L is the conductor length and A is the cross-sectional area of the conductor. Note that the resistivity, ρ , of copper (or any other material), is dependent on the temperature as described by the formula: $\rho(T) = \rho_0[1 - \alpha(T - T_0)]$, where α is resistivity thermal coefficient ($\alpha_{\text{cu}} = 0.00395\text{ }^{\circ}\text{C}^{-1}$, corresponding to an increase of approximately 40% in resistance for every increase of 100 $^{\circ}\text{C}$), and ρ_0 is the reference resistivity at ambient temperature T_0 . Now, the conductor length L , to achieve the resistance of 9.1 Ω , can be computed:

$$\begin{aligned} L &= (R \cdot w \cdot h) / (\rho_{\text{cu},20} [1 + \alpha(T - T_0)]) \\ &= (9.1 \cdot 0.267 \cdot 0.035) / (0.0175 \cdot [1 + 0.00395 \cdot (T - 20.0)]) \\ &= 4852\text{ mm} \end{aligned}$$

With the objective of achieving a higher temperature homogeneity, we chose to design the heater pattern based on a Hilbert space-filling curve (Charan et al., 2020). A Hilbert fractal can be created by the iteration of replicas of a "seed" geometry that can be rotated, or not. Fig 3.5, illustrates this process, where the final heater pattern is generated by a 6th order Hilbert curve. To create a space-filling curve with the necessary length ($L=4852\text{ mm}$), the segment size of the curve should be equal to $L / (4^{\text{order}} - 1) = 4852 / (4^6 - 1) \sim 1.185\text{ mm}$ (Fig 3.5 encircled detail).

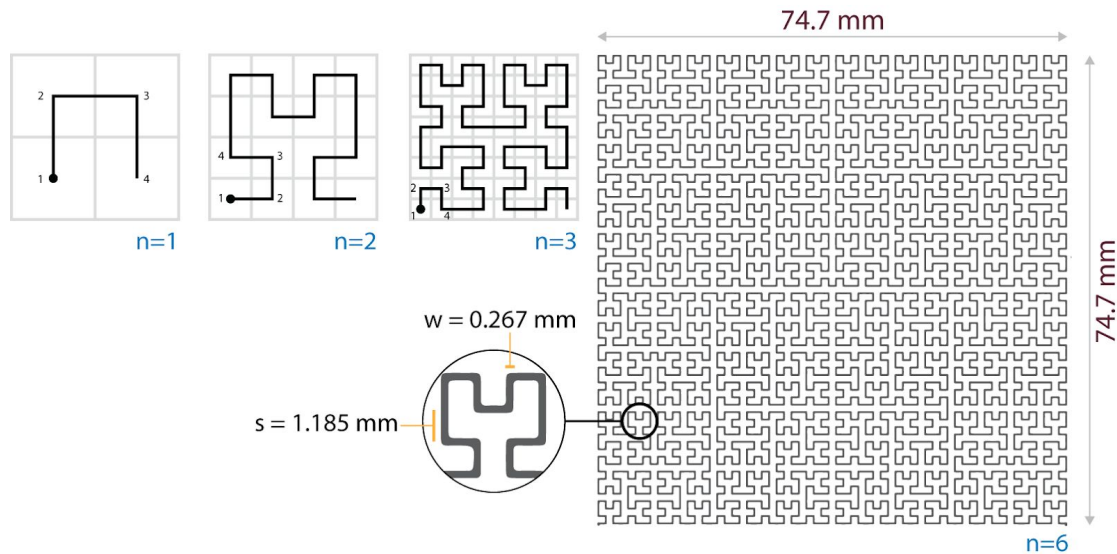


Fig 3.5: Hilbert space-filling curve used to create the planar thermal actuators. The top left section of the image shows the “seed” geometry (order 1) for the fractal and its iterations of order $n=2$ and $n=3$ (adapted from Sagan, 1994). The curve of order 6, in the right portion of the image, is the final heater geometry corresponding to an electrical resistor of 9.1Ω .

We implemented an initial prototype to test the manufacturing of these thermal actuators. We tested two target resistances on a single PCB, which also featured power delivery and temperature sensing (thus enabling feedback-based setpoint control). The parameters are detailed in Table 3.2.

Table 3.2: Parameter details for Hilbert-based thermal actuator evaluation

parameter/property	Resistor 1	Resistor 2
Track length	5528 mm	5119 mm
Trace width	0.203 mm (8 mil)	0.356 mm (14 mil)
Target resistance	13.6Ω	7.2Ω
Density of vias	64, 32, 0, 32 vias	64, 32, 0, 32 vias
Measured resistance ($n=5$ PCBs)	{8.99, 13.07, 10.18, 15.03, 7.97} Ω	{5.51, 6.76, 5.50, 7.45, 5.10} Ω

The manufactured board is shown in Fig 3.6. Under testing we were able to confirm that the heating is reasonably uniform across the actuator; and that the density of vias used did not have a significant impact on temperature reached in different areas on the reverse side. The measured variability in resistance is fairly large: for target 7.2Ω , the values have mean 6.06Ω and range from 5.10Ω to 7.45Ω ($n=5$); for target 13.6Ω , the values have mean 11.05Ω and range from 7.97Ω to 15.03Ω ($n=5$). We expect this variability to be due in part to the high manufacturing tolerances from the cheap prototyping service used. The process quality

specified for the final v2 PCB design is lower tolerance (see Sec 3.2.1). Since the temperature control will use measurement feedback, and not be based on regulating input current or voltage, some variability is nonetheless manageable.

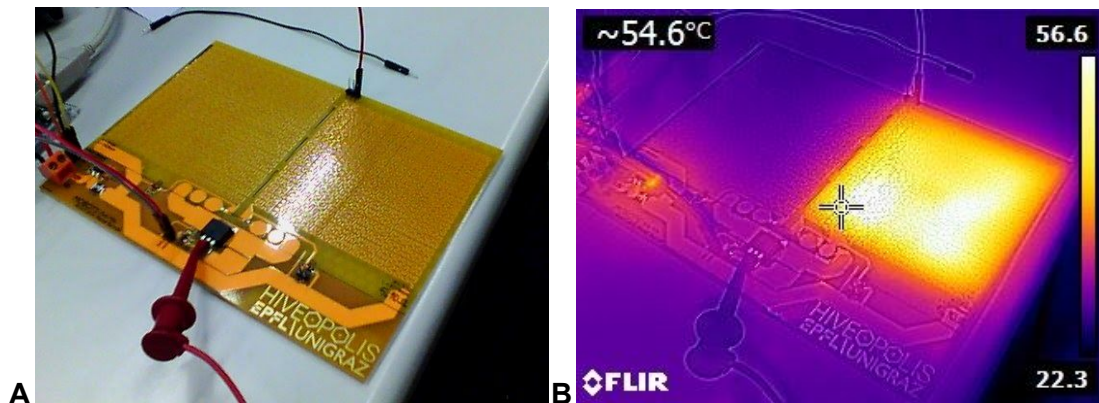


Fig 3.6: Prototype board for evaluating space-filling curves as thermal actuators. A) assembled PCB. B) Thermal image with one $7.2\ \Omega$ actuator switched on.

3.2 The second brood nest module design

Here we bring together the improved elements described above into a complete design. This includes: (1) a PCB featuring the temperature sensor array, multiple thermal elements, supporting electronics (power, storage, a microcontroller, etc); (2) a mechanical housing for the PCB to facilitate an overall brood frame; (3) the architecture for a complete test-bench: the observation hive, power supply, camera system for ground-truth data, and computing system for data logging.

The system architecture including sensors, actuators, storage and main control, is shown in Fig 3.7.

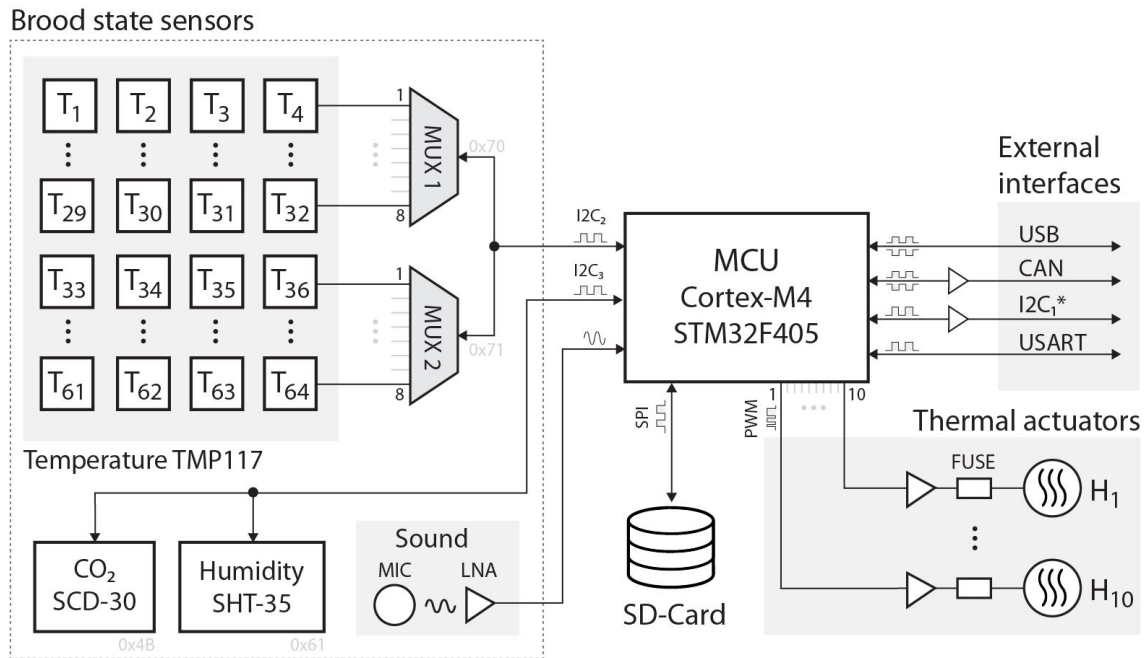


Fig 3.7: Brood nest PCB system architecture. The processing and control of sensors, actuators, and local data storage is handled by an STM32 microcontroller. The board features two banks each of 32 sensors addressed through multiplexers, and 10 thermal actuators driven by PWM outputs. The external interfaces include a custom I2C channel, which follows the signals of I2C protocol but is driven at 12 V to improve signal reliability and range (and therefore departs from the standard). This PCB is thus complemented with a down-converter (see Fig 3.11) to restore signal compliance and enable any I2C-compatible device to communicate with the system.

3.2.1 PCB design

In this section we describe how we take the specifications determined above into a unified PCB design, to provide sensing, actuating, and to form the backbone of the comb foundation.

As established in the sections above, the brood nest frame will feature 55 temperature sensors in 5 rows of 11 elements, and ten thermal actuators. Besides the temperature sensing, we also include instrumentation for CO₂, humidity, and sound measurement. In addition the system requires an RTC for reliable timestamping of data, and local data storage. Regarding IO, the basic requirements come from the peripherals and from the off-board communications. The sensors and multiplexers all use I2C, local storage (μSD card) is via SPI, the heat actuator control uses PWM outputs; the external interfacing standard will depend on the core design, which has not been settled across the project consortium, but to facilitate compatibility we here provision for multiple candidate interfaces. Given these requirements, we find the STM32F4xx family of microcontrollers (MCUs) and select the STM32F405.

Since honeybees are highly sensitive to temperature, the system should not generate excessive heat in areas that the bees can get to (with the obvious exception of the heat

actuators when active). To service this requirement, we thus organise the PCB into two zones: a bee-accessible zone, and an electronics zone. This separation should also help with minimising corrosion or other damage to the components.

The Zander frame has dimensions of 420 mm x 220 mm, and our PCB is 415 x 215 mm to allow for a supporting frame to house it (see Sec 3.2.2). The electronics zone is a 30 mm strip along the top of the frame, which will be enclosed to maintain a separation from the bees. We include an infra-red LED that can be used as a registration marker by the imaging system (for both timing and localisation). Within the bee-accessible zone, one surface is used for the heating actuators and the other surface is used for the temperature sensor array. Both of these surfaces will be covered using a bee-safe conformal coating, in addition to the 1 micrometre gold coating on all the PCB used to avoid oxidation of the exposed tracks and pads.

Given the density of routing required to reach a large number of sensors and other peripherals in the electronics zone, the PCB uses 6 layers. Its finished thickness is 1.6 mm, in order to provide some rigidity and support the comb weight. The assembled PCB appearance is depicted in Fig 3.8. The schematics files are provided in Appendix C, and detailed layout of sensors in Appendix D.

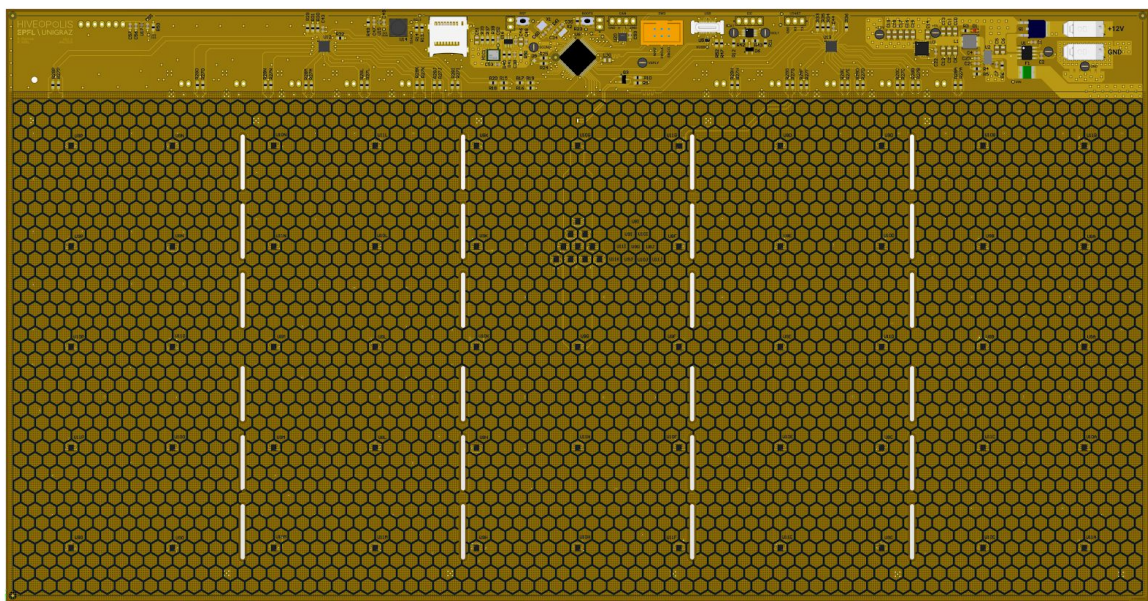


Fig 3.8: 3D render of the PCB (top side). The bee-accessible zone features a honeycomb silk-screen print, while the electronics zone at the top houses the majority of electronic components.

By choosing the STM32F4 part as the MCU, we saw an opportunity to include one extra modality of sensing that was not previously in our key specification: audio. The MCU renders this inclusion simple, and given the reports of detecting various colony dynamics with the auditory spectrum (either alone (Lima et al., 2019) or in conjunction with other sensor modalities (Rangel & Seeley, 2008; Ferrari et al., 2008)) we decided that the technical investment was merited.

To provide some isolation between the thermal actuators we include 1.5 mm x 20 mm cuts in the vertical direction (thus improving the independence of each actuator, but avoiding too great fragility of the board). The 10 actuators are placed in two rows and use square shaped elements of side 74.7 mm with an horizontal spacing of 6 mm, as shown in Fig 3.9. Heaters are powered by the main 12 V source and modulated by the MCU that controls a gate driver connected to a power MOSFET transistor.

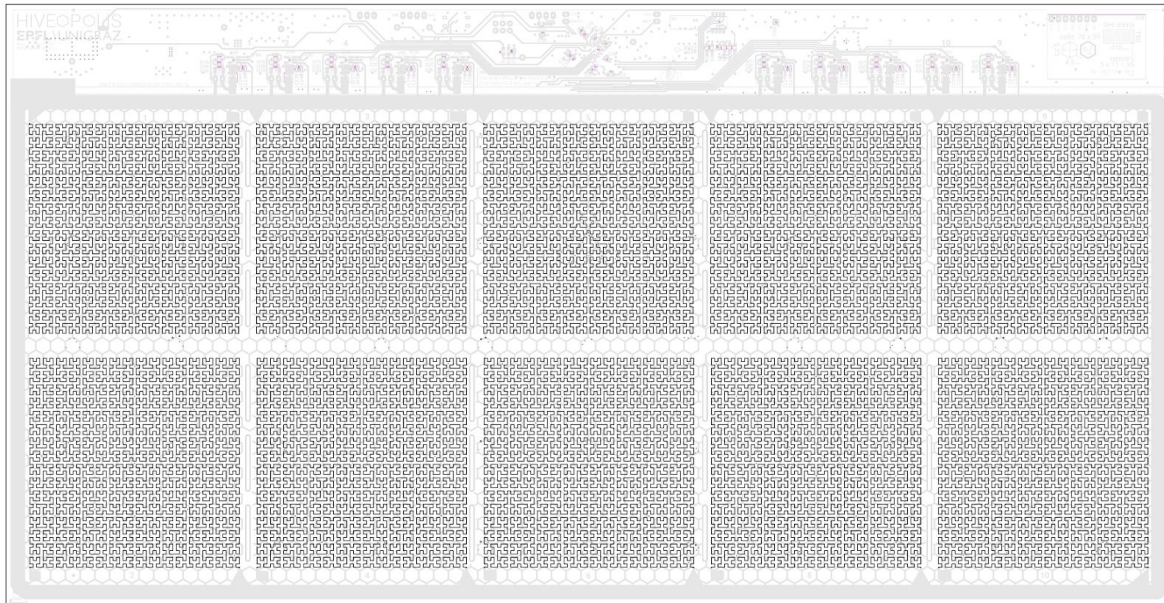


Fig 3.9: Position of the 10 thermal actuators on the bottom side of the PCB.

The selected supply voltage to the board is 12 V, which is used directly to drive the actuators. The PCB includes a switching regulator to down-convert the voltage to 5 V and an additional low-noise linear regulator to 3.3 V for the MCU, sensors, and other circuit parts. The I2C used for external communication uses a bi-directional buffer to amplify the signal to 12 V for better reliability and range (more immunity to noise), as shown in the full system diagram Fig 3.11.

Overall, this design aims to address several biocompatibility issues that we identified in the first prototype (Chap 2): using smaller sensors with lower energy consumption; removing the air-cavity between the two comb surfaces used by the bees, and better isolating the electronics from the bees. At the same time, it aims to improve performance, in terms of reliability and sensing precision, to better monitor the state of the brood.

3.2.2 Frame to house PCB

The idea behind this design is the reusability. The goal is to be able to use the same frame to support one of multiple PCB designs of the same size – different iterations of the brood nest module or prototypes from other modules. Moreover, the dimensions should fit a standard Zander hive. The concept is basic: the frame has a groove on each of the side

parts and the lower part that guides and holds the PCB. The top part is designed in such a way that it covers the electronics (visible in Fig 3.10 (c)) in the top region of the PCB, to protect it from the bees.

All of the parts can be assembled together and disassembled. The side and lower parts are glued together to make sure that the frame is resistant enough to hold the PCB. The PCB is slid into the top part from the side, and then put into the groove. We can then pin the top part with the rest of the frame by clamping the triangular parts at the top of the top part (Fig 3.10 (a) and (b)).

Regarding the dimensions, the frame corresponds to the Zander standard. Since the frame should not cover the heating zones of the PCB, its width can be directly derived from the PCB dimensions. The first prototype will be made out of Plexiglas (PMMA GS) for it is robust, not too expensive, bee-compatible and transparent. It will allow us to observe the experiments more efficiently. For the final design, we will evaluate various materials, considering in particular that it needs to support the PCB that is heavy, and the weight of the wax, honey and larvae that bees are going to place on it.

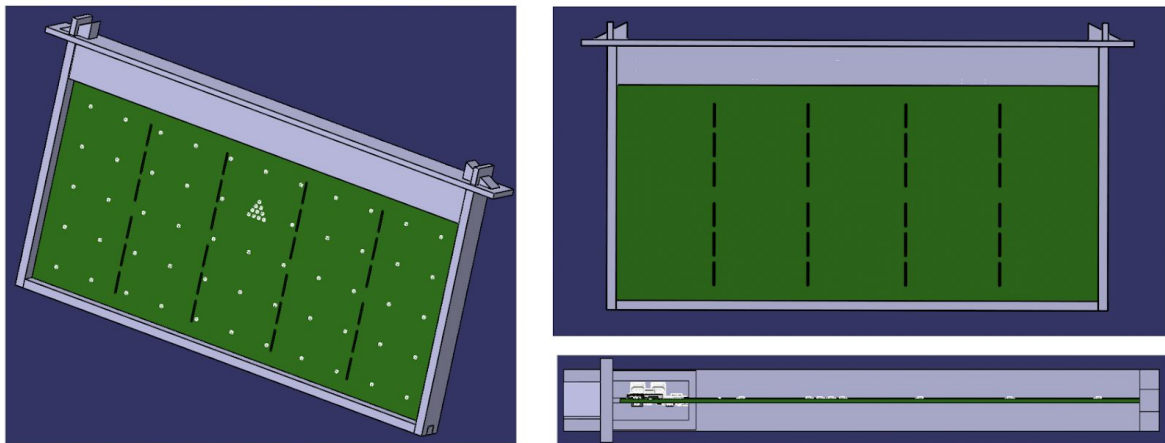


Fig 3.10: Mechanical design for frame housing : (a) Perspective (left), (b) front view (top-right) and (c) side cutaway (bottom right).

3.2.3 Full setup architecture

We bring together the components and building blocks as described above into a complete prototype design for the brood nest module. It comprises the bio-hybrid frames, the visual observation system and synchronisation between the two embedded systems, as well as large-volume storage (particularly for the image acquisition). The elements of the system are depicted in Fig 3.11 and a preliminary mechanical construction is shown in Fig 3.12.

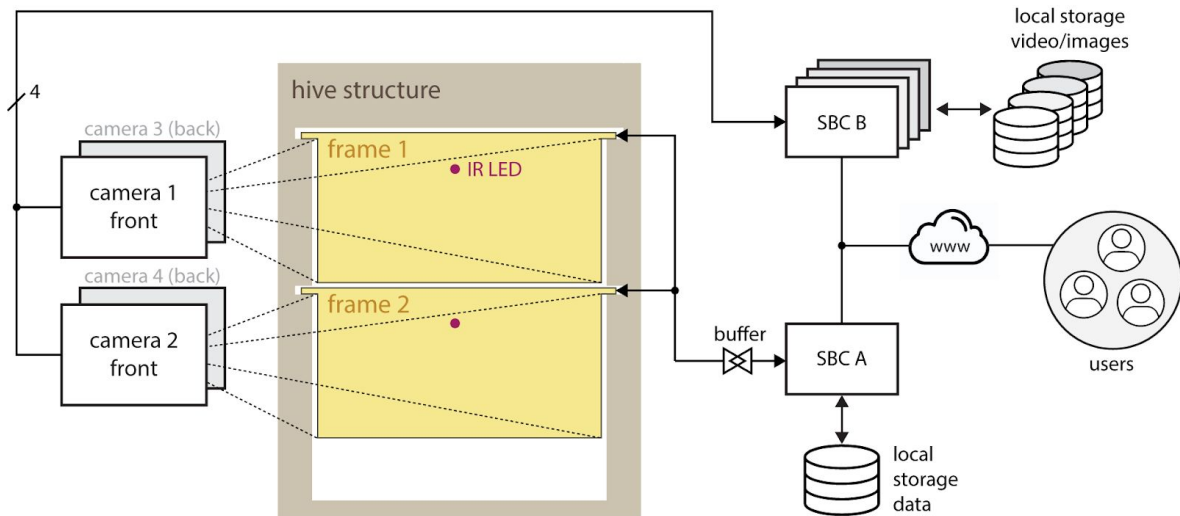


Fig 3.11: Full brood nest module system block diagram. The system incorporates an observation hive (see Fig 3.12), bio-hybrid sensor/actuator frames (Fig 3.7), a single board computer to collect data and provide a user interface to the frames, and a camera system that records each side of each frame and uses further single board computers (described in Sec 2.1.4).

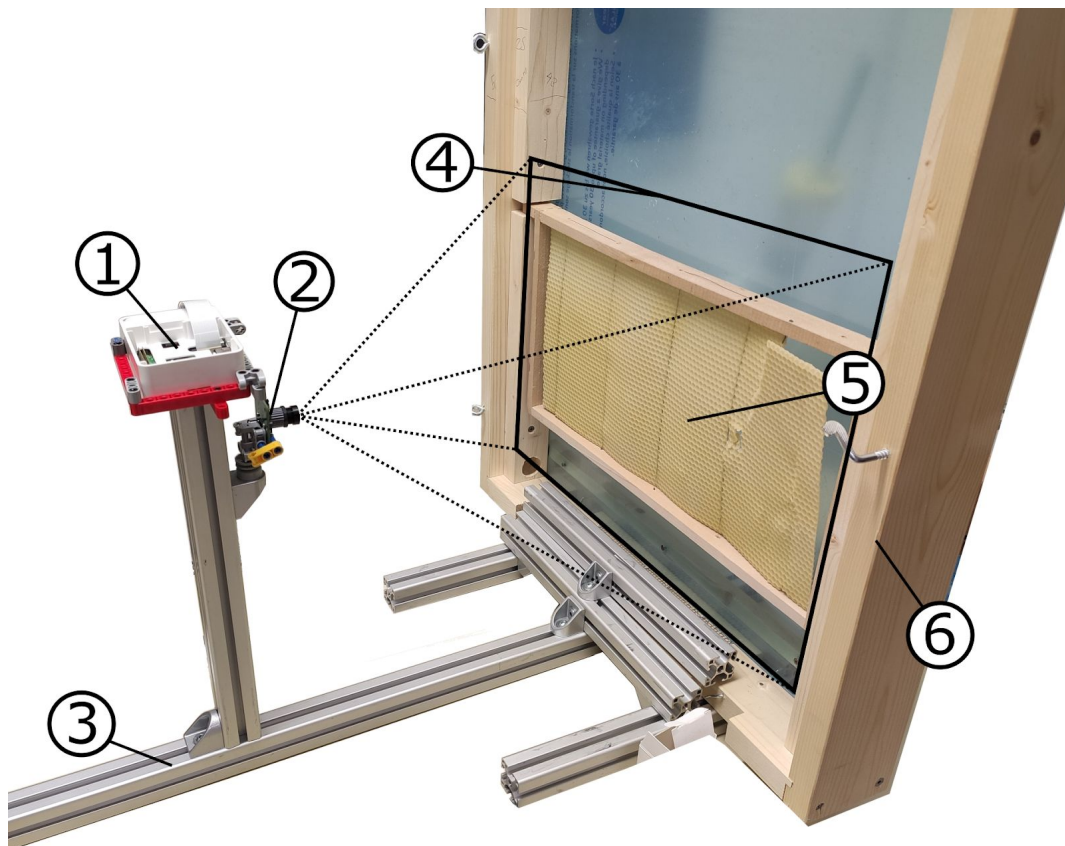


Fig 3.12: Mechanical setup of brood module prototype system, showing camera mounting with improved rigidity. 1) single-board computer to acquire and process images 2) infra-red camera 3) scaffolding 4) field of view for camera 5) Zander frame - to be substituted by the bio-hybrid frame as described 6) two-frame observation hive.

3.3 Discussion

The second iteration of the brood nest module as described in this chapter has three main aims:

- To overcome issues identified in the first prototype
- To improve precision, accuracy, and reliability in sensing and actuating
- To facilitate closed-loop control of the actuators

We summarise technical improvements made towards these aims by this second prototype design in comparison to the first iteration in Table 3.3.

Table 3.3: Comparison of specifications for thermal sensing and actuation between initial and second prototype of brood nest module

		First prototype	Second prototype
s e n s o r	Number of sensors	88 (2 x 44)	55
	Resolution	1/16 °C	1/128 °C
	Accuracy (20°C - 45°C)	±0.5 °C	±0.1 °C
	Precision	Not provided by manufacturer	±0.0078 °C
	Sensor dimensions	3.5 x 4.5 x 4.5 mm ³	2 x 2 x 0.8 mm ³
	Standby current	1 µA	0.15 µA
	Active current	1500 µA	3.5 µA
	Communication protocol	1-wire	I2C
a c t u a t o r	Number of heaters	4	10
	Voltage and max. power	12 V / 20 W	12 V / 15 W
	Dimensions	190 mm x 190 mm x 3 mm	74.7 mm x 74.7 mm x 35 µm

The integral PCB that features arrays of temperature sensors and thermal actuators is at the centre of achieving these aims. Specifically, the PCB design aims to address several biocompatibility issues that we identified in the first prototype (Chap 2): using smaller sensors with lower energy consumption; removing the air-cavity between the two comb surfaces used by the bees, and better isolating the electronics from the bees. At the same time, it aims to improve performance, in terms of reliability and sensing precision, to better monitor the state of the brood. Moreover, the actuator array is now under computer control, making it possible to connect the actuator states to brood state information derived from the sensors. We have also made crucial advances in the software and mechanical setup of the camera system, which should facilitate more robust ground truth data collection.

Besides the developments in design, the data gathered during the 2019 season led us to some interesting observations, both in the temperature array data, the image series, and the combination of the two. The analyses presented in this report are preliminary, and we anticipate being able to identify more concrete explanatory relationships with further developments in our analyses. For example, it will be interesting to compare the activity trajectories between the two brood frames, to examine whether the subset of data used per day was a suitable sample for extracting longer-term trends or whether the complete data offers more. Bringing together the data from the two different streams more rigorously is an important future direction, and we will also consider measuring the environmental conditions within and outside the observation hive room, and also the local weather, to better establish what data are most informative for brood state and for prediction of future dynamics.

Chapter 4: Integrated camera system for brood nest observation and mite infestation assessment

4.1 Importance of larval observation

One basic element to assess the health status of a colony, as well as predict its future status, or detect changes of the developmental dynamic, is the detection of variance in the growth process of its larvae. The parameters that are interesting for this topic are (Fig 4.1, right):

- Total length of the larva;
- Diameter of larva at defined points;
- Opening angle of larva;
- Point in time when the larva “closes the loop”, i.e., when one end touches the other end;
- Shape and size of the “eye” that forms after the larva have closed the loop;
- Variations in all the mentioned parameters within the population.

To collect these parameters we developed and tested an experimental setup, hereafter called: “the camera module”.

Observations of growth and behaviour of larvae in the cell over time were conducted with four cameras to obtain in-hive pictures.

To understand how bees treat their larvae under several environmental conditions it is necessary to have a tight observation regime, not only in a spatial manner, but also in temporal scales. With this you could track the growth and development of single larva and determine the overall health state of the bee colony.

Furthermore, one highly relevant parameter for the health assessment and the future wellbeing of the colony is the intensity of mite infections. This shall include, for example, the numbers of infected cells, the number of mites per cell and the amount of cleaned cells that were infected.

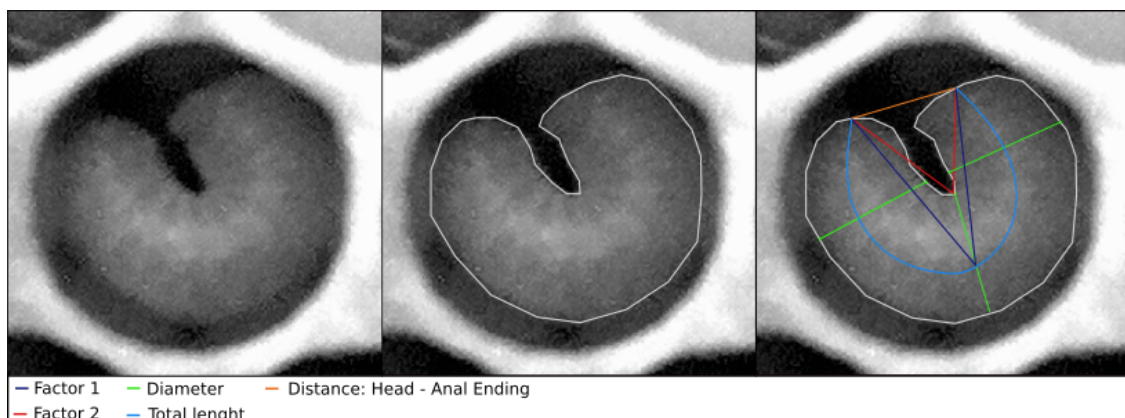


Fig 4.1: Scheme of planned image processing. Right: Color changed larva. Middle: Framed outer limits of larva. Right: Parameters to take to get sufficient information.

4.2 Functional constraints

According to the general plan of the HIVEOPOLIS system we aim to fulfill a set of constraints that could be of relevance for the final HIVEOPOLIS hive (see Table 4.1).

The visual, non invasive observation of the growth and development of larvae was tested in a full hive (Zander measure). The system should be designed to fit between the brood combs but minimise disturbing effects for the bees. As there is no external power supply at the test hives, a local power supply has to be included and the selected electronics are dimensioned so that the overall energy consumption is as low as possible. The lack of WiFi at the hives also suggests a local data storage. Summed up, this means that the camera system needs to be autonomous and a closed unit.

Table 4.1: Detailed constraints of the camera module, as set by the overall goals of the HIVEOPOLIS system; for more details see Deliverable D2.1 (Functional requirements of the system)

Energy autonomy	The integrated camera module should be able to operate with very low power consumption over several days.
Non invasive	The observation should not disturb the natural structure of the colony. Therefore the camera module should be minimal in size. Emissions of light, heat and vibrations should not change the in-hive situation. Toxin security should also be considered in the choice of materials.
Offline	The HIVEOPOLIS system should theoretically be able to operate in areas without power supply or connection to the internet.
High resolution	Observations of larvae growth processes and mite infection status of several larvae in parallel is one of the main tasks of the camera module. Therefore it is necessary to use several cameras that observe several larvae on one brood comb.

4.3 Implementation

To achieve the goal of an integrated camera system and to test it in a full colony, a casing that fits into a full hive with Zander measures (420 mm x 220 mm) was built. The width was chosen with 60 mm. This is two combs, 25 mm each, plus 10 mm. The frame was made from spruce, the front from common 4 mm window glass and the background from foamed PVC. Ventilation holes were drilled in the top and bottom of the frame and covered with wire mesh. The wire mesh kept the bees from getting into the module (Fig 4.3). All of the components were mounted on the backplate, first with nails and later with screws. It contains the single-board computer, cameras, light, power source and data storage (Fig 4.2).

4.3.1 Hardware design

For processing, the RaspberryPi 3B+ was chosen as it has an onboard graphics unit making it well suited for use with cameras, and an integrated WiFi module. The multiplexer, to address the four cameras, is from ArduCam©. An external clock and a 32 GB USB-Stick for image storage were also mounted on the RaspberryPi.

Common red LEDs with a wavelength of approximately 700 nm were used as a light source, as the emitted light is invisible to bees. Infrared LEDs (wavelength > 760 nm) would be fitting as well, but have a higher energy consumption and were therefore discarded as a viable option. Five LEDs were soldered on a board and made one light unit, of which a maximum of three were used.

The system's energy is provided by a 26000 mAh power bank and an additional fuse was installed at its output.

A relay with a timer activated the system in recurring periods. The relay needed a separate energy source as modern power banks have shut down automatically when the drawn current was under a certain level for a certain time. The timer and relay seem to stay under this threshold, so an old power bank with 2400 mAh was used as the energy source (a pack of batteries also could have been used instead).

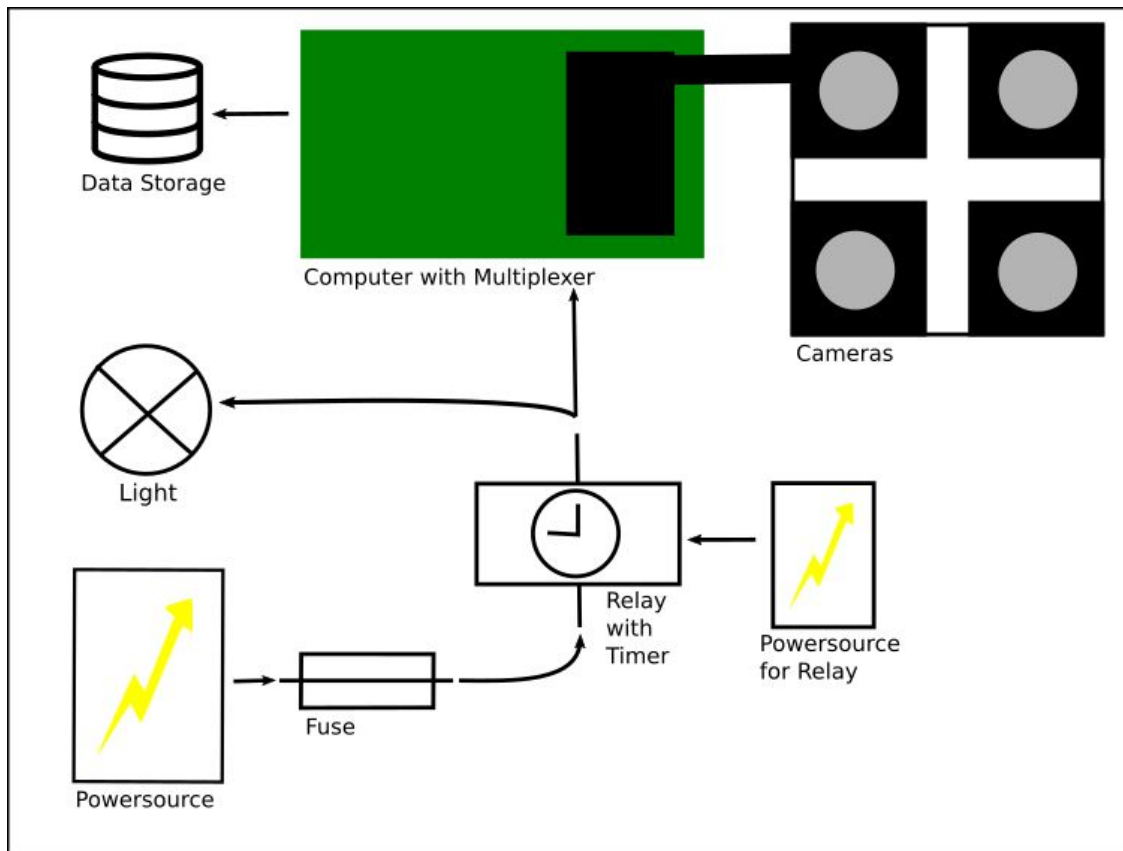


Fig 4.2: Schematics of the hardware setup with all parts that were built into the final version of 2019. The main improvement was the relay with the timer.

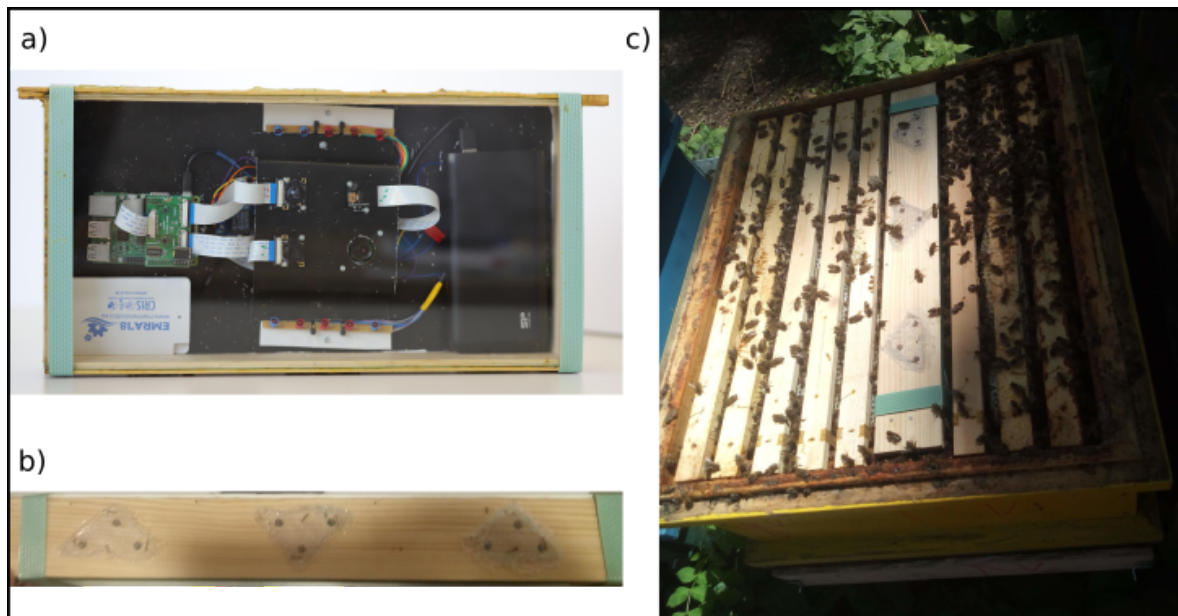


Fig 4.3: a) Fully assembled Camera Module (final Version 2019) b) Holes in the top and bottom to enable air circulation and heat dissipation c) Camera Module integrated into a standard hive.

4.3.2 Software

All software that was used is open source. As an Operating System for the RPi, the official Raspbian Buster was installed. The needed software to use the ArduCam Multiboard is provided by the company. After the start up of the system a daemon-file, made in systemd, started all necessary processes to take images. A VNC server was activated after start up to make it possible to connect from outside the hive. The cameras were operated with the Raspberry Pi software utility “raspistill”, managed by a python script.

4.3.2 Development over time

During the developmental process of the camera module, 3 prototypes of increasing complexity and features were built (Fig 4.4).

The first version was very simple and quickly assembled to test the overall concept of the integrated camera system. An initial wooden backboard was replaced by foamed PVC for easier mounting and changing of components.

In the second version, the arrangement of the parts was improved and an additional level was added to reduce the distance between the camera lens and the comb. Additionally, to be able to append a timestamp to the images, an external clock driven by a button cell was assembled. The IR lights were powered by the GPIO pins, not directly by the power source.

The power source for the lighting was changed in the 3rd and latest iteration of the season in 2019. A relay with a timer was introduced, which made it possible to restart the RPi every recurring cycle and to power the lights with the power bank. This saved a lot of energy and the runtime of the experiments were extended to 3 days. However, this approach required a second (smaller) power source for the relay.

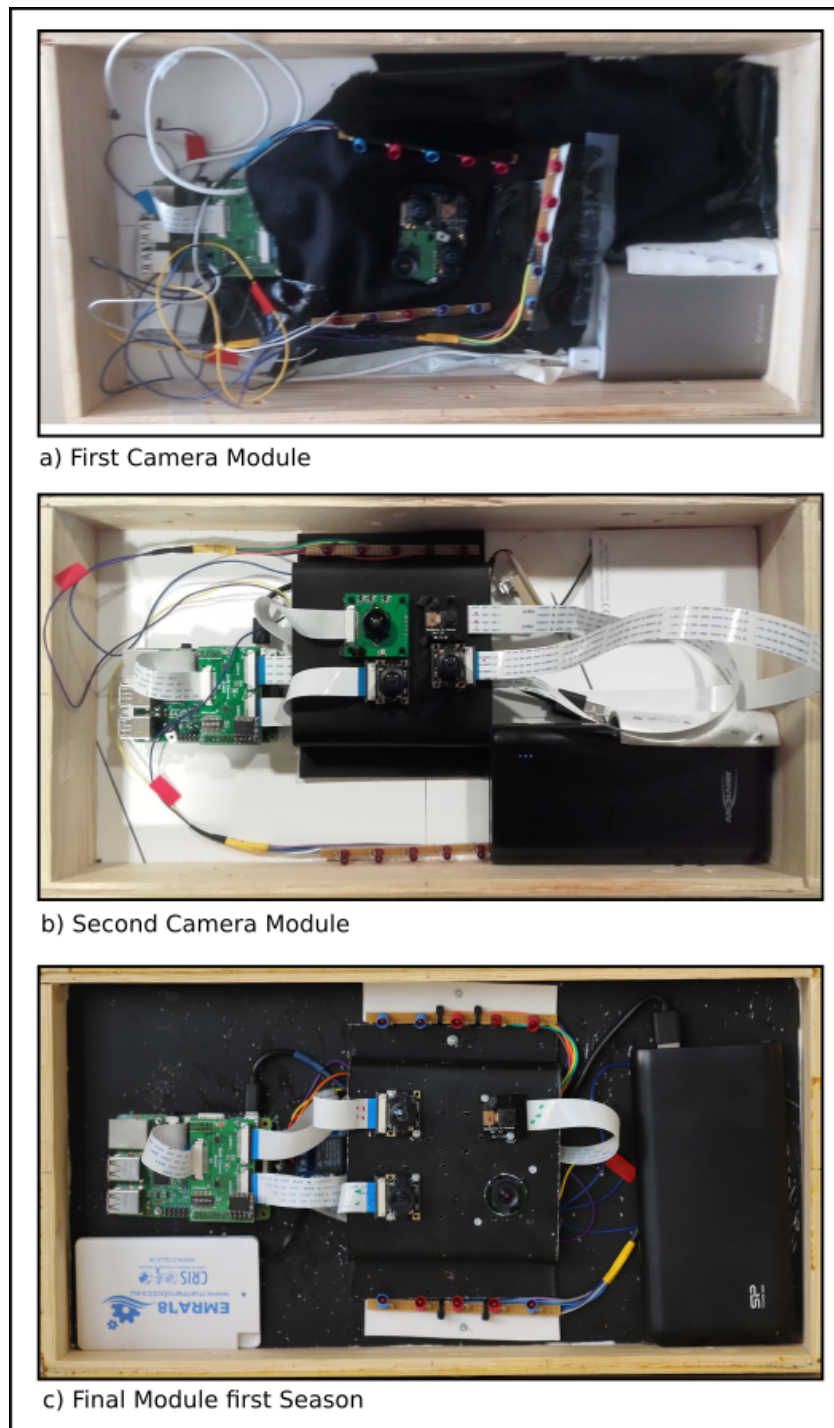


Fig 4.4: Evolution of the Hardware design of the camera module over time. Figure a) shows an early version with one power bank. The main purpose was to test the software features, control methods and runtimes. Figure b) shows the second version with improved camera mounting (centre) and improved localisation of light. Figure c) shows the latest camera module prototype with several improved features.

4.4 Performed tests

To find the best camera and configuration for observing larval development, tests with different cameras of different focal lengths and photosensitivity were performed. To identify which of the many available cameras for RPis provides the highest quantity of visible cell floors, several were tested:

- Arducam, 5MP, OV5647, Fisheye LS-40190 Lens
- Arducam, 5MP, OV5647, horizontal field of view of 56°
- RPi Camera module, V2, 5 MP, 160° wide angle, NoIR
- RPi Camera module, NoIR, V2

The OV5647 is a 5 Megapixel CMOS chip from OmniVision and the V2 a 8 Megapixel Sony IMX 219 CCD chip. We used 4 different cameras at once in the final module.

The tests were conducted during the whole experimental season (May - October 2019). The goal was to take 10 to 20 pictures every three hours, with each of the four cameras, for a maximised time span. The longest experiments lasted for approx. 72 hours, with the energy supply of the relay being the limiting factor.

4.5 First results

As a result of testing the camera module inside a hive of a full colony with different settings and cameras, a broad variety of different situations can be shown. Starting from an overview of the surface of the comb, produced with a camera with fisheye lens, to a very close and detailed picture of larvae with the Arducam (Fig 4.5 - Fig 4.11).

Increasing the distance between the cameras and the comb would reduce the parallax shift, but as we have to operate in a small margin of possible distances to meet the upper size limitation requirements of the module the required increase in the distance to get rid of parallax effects altogether would be too high. Additionally, being closer to the brood led to acquisition of higher levels of detail of the larvae themselves.

One big problem was the provision with light. Due to the very low light intensity, camera parameters had to be adjusted. The changeable camera options were ISO, shutter speed and exposure time. Because of the bad light conditions exposure times were set to 4s - 6s, and ISO values between 400 and 800. The long exposure led to “blurry” pictures and bad sight of the larvae, as there were adult bees constantly running around the brood nest.

Honeybee larvae were observed in every stage of their development (Fig 4.12). Depending on cameras used in different resolutions, the capped cell is more blurred as the focus of the camera lenses is on the cell floor.

Pictures taken every three hours over the lifecycle of a single larva could be enough to track the changes in a sufficient manner (Fig 4.13).

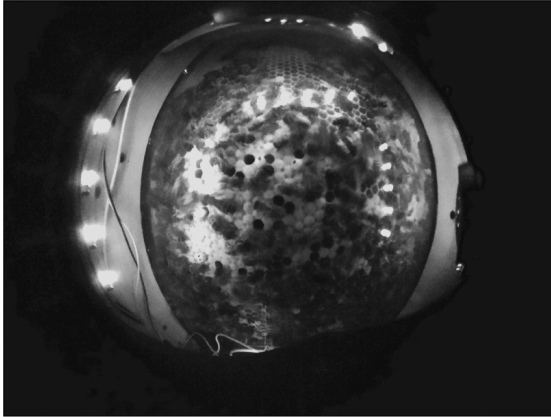


Fig 4.5: Arducam 5MP OV5647 Fisheye LS-40190 Lens Camera Module. Good overview of one third of the comb.

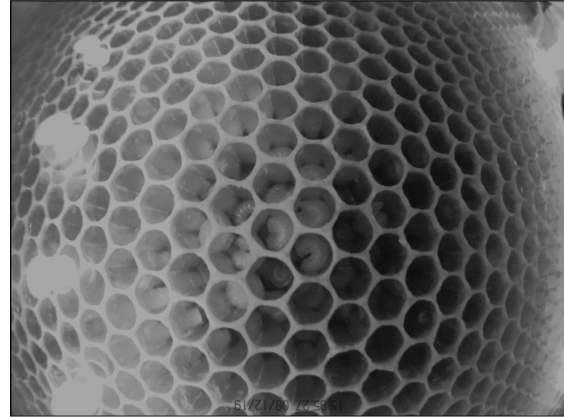


Fig 4.6: RPi Camera module, 5 MP, 160° wide angle, V2. No adult bees shortly after treatment with oxalic acid.

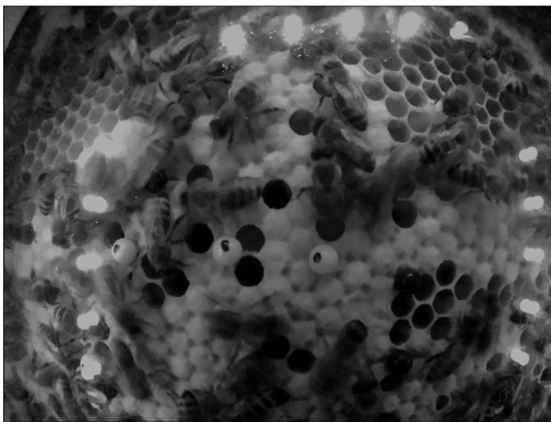


Fig 4.7: Same camera as Fig 4.6, greater distance to comb; could be used for behavioural observation; capped and open cells visible

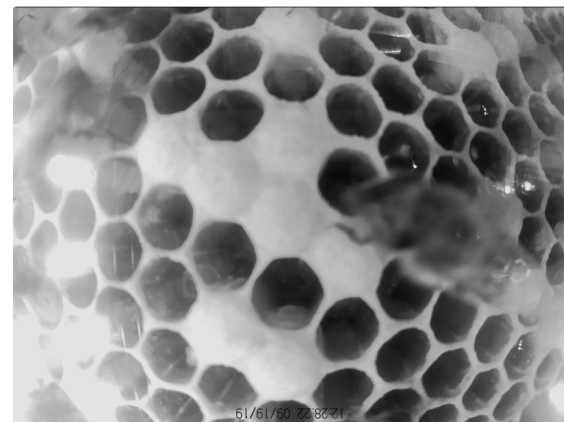


Fig 4.8: Same camera as Fig 4.6, with a smaller distance to comb

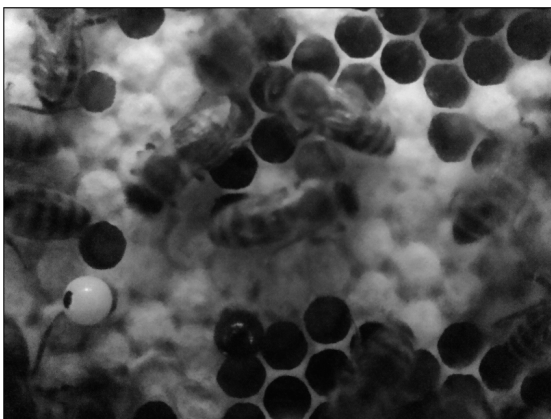


Fig 4.9: RPi camera module, NoIR, V2.; again capped and open brood cells are clearly visible

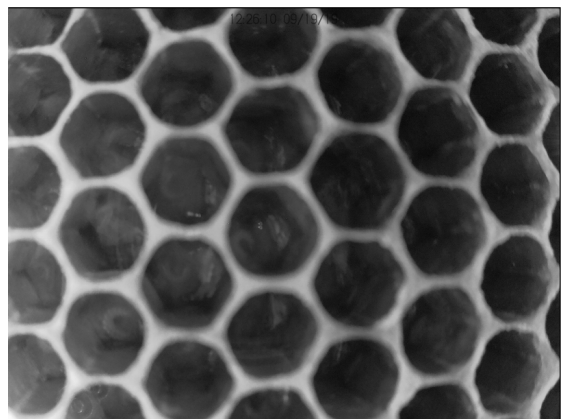


Fig 4.10: Same camera as Fig 4.9, but closer to the comb. Allows monitoring of single larva.

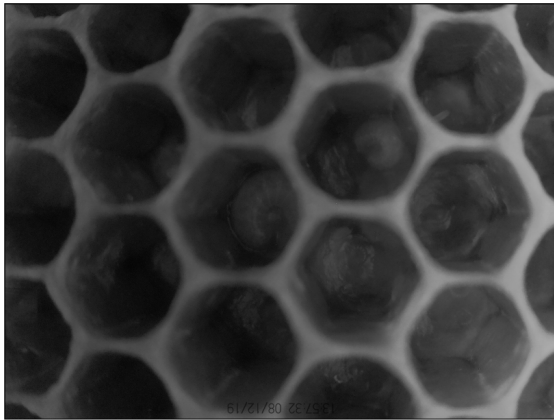


Fig 4.11: Arducam 5MP OV5647, horizontal field of view of 56°. This camera gives a very detailed insight on the larvae.

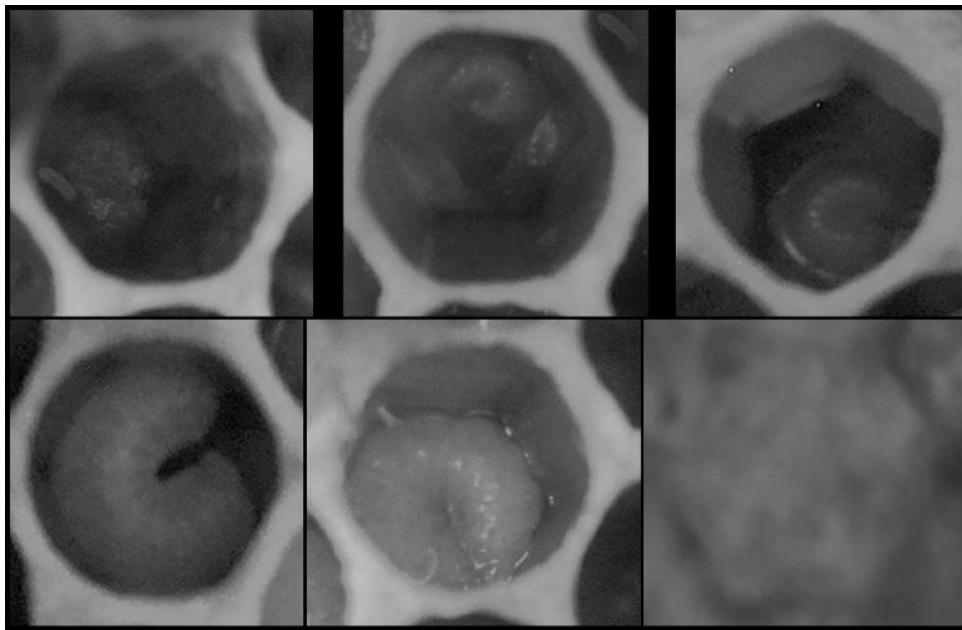


Fig 4.12: Important stages of honeybee development. From egg to capped brood. Pictures are from different cameras in different test runs.

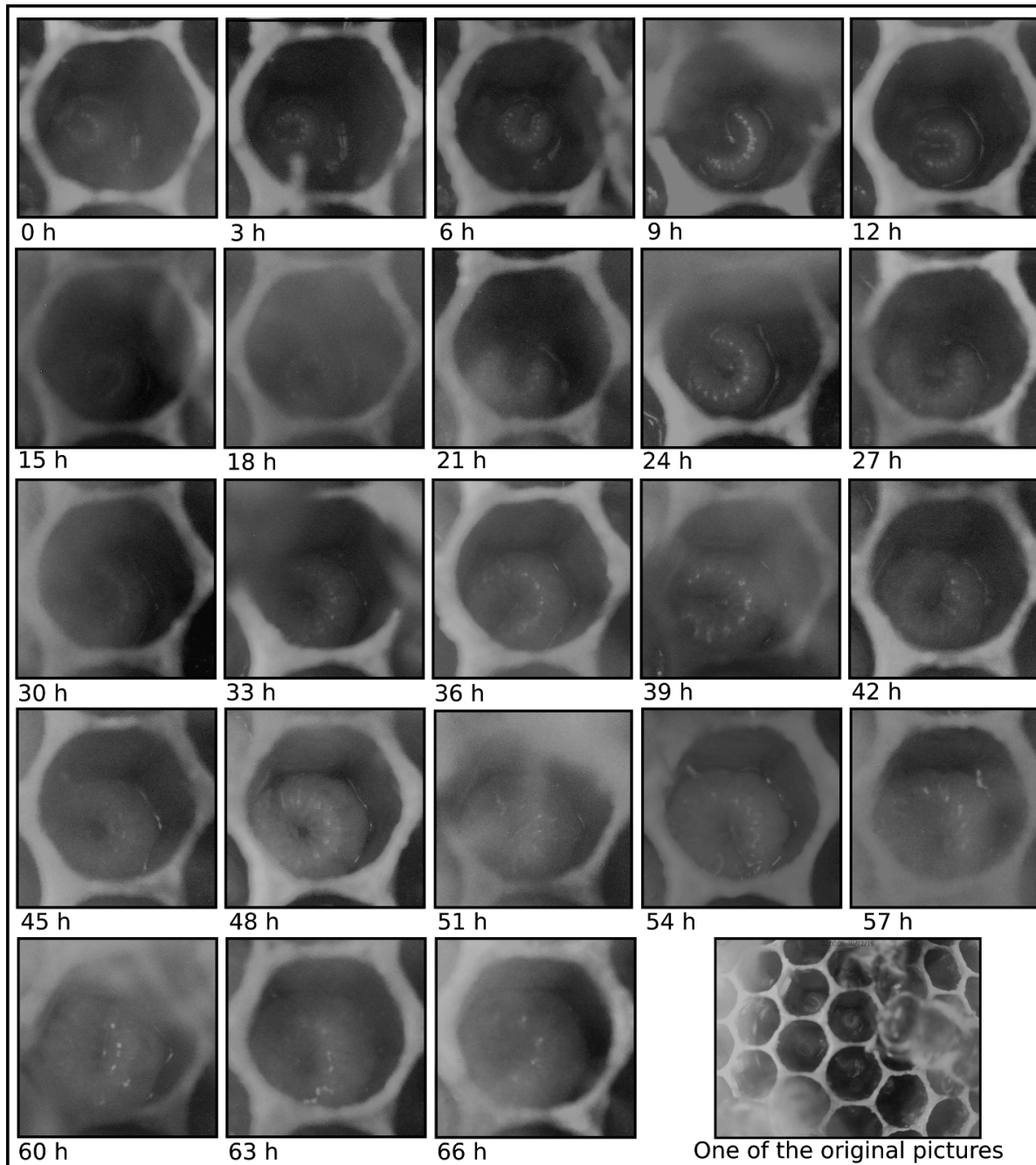


Fig 4.13: Exemplary time series of one individual larva over 66 hours.

The following hardware settings and elements seem optimal for the task defined in the functional constraints (Sec 4.2):

Camera: We found that a camera chip with 5MP resolution is adequate for the purpose of brood observation. Depending on the constraints and goals we tested multiple optical lens types, ranging from fisheye (angle of view: 180°) to wide angle (AOV: 63° - 114°) and normal angle (AOV: 44° - 53°).

Size: The doubled comb width seems to be an optimal size, as it has only a small influence on the colony, is only a little invasive (compared with other approaches, e.g. a classical observation hive) and has enough space for the required hardware.

Time regime: A series of 10 to 20 pictures with a temporal delay of 35 seconds taken every 180 minutes gave us a satisfactory number of pictures and allowed us to follow the development of individual larvae in a sufficient temporal resolution. It is necessary to take a series of images with several seconds delay for the simple reason that bees move over the comb. To get a clear picture of a larva it is necessary to pick either one where no bee is above the larvae, or to computationally remove the bee by comparing several images with a relatively short time delay. The length of this delay is tricky, for on the one hand it should not be too short, so the bees can find time to move away, but also not be too long, else the movement of the larva can harm the chance for a mathematical refinement of the image. The found image delay of 35 seconds, and 20 Images per series was found as a best practice so far. The delay between the series of 180 minutes allowed us to get enough information over time to efficiently observe the growth process.

4.6 Conclusion on the camera module

4.6.1 General conclusion

The work described in this chapter showed that the developed camera module is highly suitable for observation of the growth process. As the system can operate autonomously over several days it allows the observation of individual larvae development, a process that typically lasts for 21 days from egg laying until the cell is capped.

The Raspberry Pi camera module with a 5MP chip and a 160° wide angle lens is also suitable for varroa observation, for it can see into the cells as well as give an overview. The moment of varroa entering the cells happens shortly before capping and can likely be determined, although it would also be important to observe the hygienic behavior of nurse bees in an infected hive for that purpose. The full capability of the proposed system is to be tested in long run experiments in future seasons.

4.6.2 Advantageous hardware settings and design paradigms identified

Although the results seem to be satisfying it is necessary to point out that the camera module at hand is currently a very early prototype. The following elements and design decisions are candidates for refinement:

Raspberry pi B model for main control purposes: Although the RPi is a widely used low power computer it is maybe not the optimal choice for the task of low power long term observation. Other hardware boards (e.g., RPi ZERO) that have an even lower power consumption but still fulfill the needs and constraints are candidates that may improve our camera module.

Single controller design: At the moment, one controller (in our case a RPi) can read data from 4 cameras. Theoretically this can be extended to 16 cameras. It is to be discussed, if an approach with a single controller device with 16 cameras is more feasible than the idea of using several controller units with 4 cameras each of which would lead to higher parallelism.

Energy and information autonomy: Running the proposed system purely offline, with a low- or zero-power regime, massively limits the possible capabilities of the system. It could be useful to rethink if full energy autonomy is necessary. Even with small amounts of constant power supply, the suggested camera system could operate with much higher efficiency. Same holds for “in-system” data storage. The module produces about 4 Gigabytes of data per day (despite the fact that the amount of images taken was reduced to the usable minimum with 10 images per camera per sequence; a sequence every 3 hours, with 4 cameras per module). Therefore the possibility of data transfer would be advantageous.

Light situation: One parameter setting that has high potential for adaptation to a given experiment is the light situation. More light produced by the module leads to less exposure time, which reduces the calculation time of the main module. This would allow us to take more images over time. The downside of more light is the possible influence on the temperature and heat dissipation, and hence on the behaviour. In the experiments described above, the light intensity and the number of light sources were chosen to allow us to produce usable images, but in parallel to minimise the change in temperature which may be influencing the colony.

Camera positioning: The position of the cameras, especially their distance to the comb, as well as the distance between themselves has a big influence on the data quality. Specifically, the closer the camera is, the more relevant the parallax problem becomes, but at the same time the better the resolution of the resulting image gets.

Software improvements: Modern cameras allow image improvement with software tools. No such software image enhancements were used in these first prototype tests. It is plausible that using advanced software image enhancement would substantially improve image quality in the task of larvae observation.

Special glass anti mirror: The module used a standard glass. Special glasses (e.g.: anti-mirror glasses, special optical glasses) could improve the image quality, especially the used light and the resulting light situation would be adapted.

Infrared light system/monochromatic light system: The system operates with visible light. The usage of IR-cameras and light sources, or respectively monochromatic cameras and light sources could also further improve the quality of the output.

Data Compression: In the setup the images were stored on a local drive. In an advanced system, a more sophisticated compression algorithm or alternatively an automated data pre-evaluation could be used to lower the storage space constraints. This however would increase the needed calculational efforts and the trade-off with battery life would have to be taken into account.

4.6.3 Suggested future tests / future questions to be answered:

The tool presented in this chapter represents an intermediate step between the concept phase of HIVEOPOLIS, and the final HIVEOPOLIS system. With the following list we want to suggest next steps, rather than presenting a roadmap. The final way of proceeding will be influenced by the ongoing analysis of data and the ongoing technological development, which, especially in the field of microcomputing and camera technology, can be very dynamic from one year to the next.

As a first step we would see the necessity to **test several camera modules over several weeks and months** to test their stability regarding software and hardware elements, and the interplay with the colony.

Further the concept of **more cameras per camera module** is to be tested for its feasibility regarding power consumption, data storage limitations, and hardware and software system complexity issues.

One open issue from a scientific point of view is the question of **what percentage of a colony's brood area has to be observed** to get a significant overview of the condition of the colony, and the variation in the colony, be it regarding the growth of the larvae or infection with parasites.

At the moment the camera module is used to produce images. From a technical point of view, it could be possible to **use it for production of footage** for behavior observation of bees. If the quality of footage is sufficient for behavioural analysis, and how this influences the hardware constraints like power consumption, data storage limitations, etc. are questions that remain to be answered.

In comparison with classical observation hives, the presented camera module enables the observation of growth processes and behavioural observations in a classical cubic full colony, which is a much more natural condition for a honeybee colony. It is necessary to run a detailed analysis of the interplay between the colony and the observation modules, in comparison with the classical observation hives, to **check for differences and biases based on the different spatial configuration** of the experimental hives.

With a sufficient number of cameras, a **3D reconstruction** of the processes in the colony in the observed areas could be possible. If this is possible at all, and what hardware and software improvements or even which conceptual improvements are necessary to reach such a goal, should be a topic of discussions. The merit of such datasets would be that it opens doors to new levels of behavioural observation and larvae observation in full colonies, be it by man or automated systems.

From a long-term point of view a discussion should be started about whether in-colony observation modules, like the one presented here, can be used as surrogates for the classical observation hives. This is relevant because this system allows the observation of processes in a full colony, in contrast to the more artificial classical observation hives. The merit of such a step would be to get data from colonies under more natural conditions, which would allow us to observe more natural behaviours, without possible biases of classical experimental setups. For sure this step is influenced by the improvement and development of features like size, camera resolution, camera hardware technology and 3d-augmentation of the produced data.

Conclusion

Our overall objectives with the brood nest module are to be able to (1) measure the state of the brood nest, and (2) influence the dynamics of when and where brood is raised. With these two facets acting in closed-loop, our aim is to develop a bio-hybrid system comprising mechatronics and honeybees that together exhibit collective dynamics and behaviours. The system described in chapter 4 is a visual system that aims to acquire detailed imagery within-hive. The presented prototype delivers convincing results that will allow us to decide on the next steps in development of the HIVEOPOLIS system. The final brood nest module that will appear in the HIVEOPOLIS units is planned to feature a detailed imagery sub-module as described in chapter 4, a temperature sensing array, and a thermal actuator array, as described in chapters 2 and 3.

List of Appendices

- A. Brood nest sensor array density model, 8pp
- B. Brood nest bio-hybrid system components, 2pp
- C. Brood nest second prototype schematics, 8pp
- D. Temperature sensor address map, 1p

References

- Altun, A. A. (2012). Remote Control of the Temperature-Humidity and Climate in the Beehives with Solar-Powered Thermoelectric System. *Journal of Control Engineering and Applied Informatics*, 14(1), 93-99-99.
- Awtrey, D. (2004). *1-Wire design guide* (p. 95). Springbok Digitronics.
https://dutta.csc.ncsu.edu/iot_spring17/wrap/1-Wire-Design%20Guide%20v1.0.pdf
- Bauer, D., Wegener, J., & Bienefeld, K. (2018). Recognition of mite-infested brood by honeybee (*Apis mellifera*) workers may involve thermal sensing. *Journal of Thermal Biology*, 74, 311–316. <https://doi.org/10.1016/j.jtherbio.2018.04.012>
- Bayir, R., & Albayrak, A. (2016). Intelligent Control System of Intra-Frame Beehive Heater. *International Journal of Computing Academic Research (IJCAR)*, 5(4), 220–232.
- Becher, M. A., & Moritz, R. F. A. (2009). A new device for continuous temperature measurement in brood cells of honeybees (*Apis mellifera*). *Apidologie*, 40(5), 577–584. <https://doi.org/10.1051/apido/2009031>
- Bonoan, R. E., Goldman, R. R., Wong, P. Y., & Starks, P. T. (2014). Vasculature of the hive: Heat dissipation in the honey bee (*Apis mellifera*) hive. *Naturwissenschaften*, 101(6), 459–465. <https://doi.org/10.1007/s00114-014-1174-2>
- Brooks, D. G., & Johannes, A. (2015). *Trace Currents and Temperatures Revisited* (p. 48). <https://www.ultracad.com/articles/pcbtempr.pdf>
- Bujok, B., Kleinhenz, M., Fuchs, S., & Tautz, J. (2002). Hot spots in the bee hive. *Naturwissenschaften*, 89(7), 299–301. <https://doi.org/10.1007/s00114-002-0338-7>
- Charan, K. K. S., Nagireddy, S. R., Bhattacharjee, S., & Hussain, A. M. (2020). Design of Heating Coils Based on Space-Filling Fractal Curves for Highly Uniform Temperature Distribution. *MRS Advances*, 1–9. <https://doi.org/10.1557/adv.2020.17>
- Doull, K. M. (1976). THE EFFECTS OF DIFFERENT HUMIDITIES ON THE HATCHING OF THE EGGS OF HONEYBEES. *Apidologie*, 7(1), 61–66.
<https://doi.org/10.1051/apido:19760104>
- Dunham, W. E. (1931). Hive Temperatures for Each Hour of a Day. *The Ohio Journal of Science*, 31(3), 181–188.
- Edwards Murphy, F., Magno, M., Whelan, P., & Vici, E. P. (2015). b+WSN: Smart beehive for agriculture, environmental, and honey bee health monitoring — Preliminary results and analysis. *2015 IEEE Sensors Applications Symposium (SAS)*, 1–6.
<https://doi.org/10.1109/SAS.2015.7133587>

- Esch, H., & Goller, F. (1991). Neural Control of Fibrillar Muscles in Bees During Shivering and Flight. *Journal of Experimental Biology*, 159(1), 419–431.
- Fahrenholz, L., Lamprecht, I., & Schricker, B. (1989). Thermal investigations of a honey bee colony: Thermoregulation of the hive during summer and winter and heat production of members of different bee castes. *Journal of Comparative Physiology B*, 159(5), 551–560. <https://doi.org/10.1007/BF00694379>
- Ferrari, S., Silva, M., Guarino, M., & Berckmans, D. (2008). Monitoring of swarming sounds in bee hives for early detection of the swarming period. *Computers and Electronics in Agriculture*, 64(1), 72–77. <https://doi.org/10.1016/j.compag.2008.05.010>
- Giammarini, M., Concettoni, E., Zazzarini, C. C., Orlandini, N., Albanesi, M., & Cristalli, C. (2015). BeeHive Lab project—Sensorized hive for bee colonies life study. *2015 12th International Workshop on Intelligent Solutions in Embedded Systems (WISES)*, 121–126.
- Gil-Lebrero, S., Quiles-Latorre, F. J., Ortiz-López, M., Sánchez-Ruiz, V., Gámiz-López, V., & Luna-Rodríguez, J. J. (2017). Honey Bee Colonies Remote Monitoring System. *Sensors*, 17(1), 55. <https://doi.org/10.3390/s17010055>
- Groh, C., Tautz, J., & Rössler, W. (2004). Synaptic organization in the adult honey bee brain is influenced by brood-temperature control during pupal development. *Proceedings of the National Academy of Sciences*, 101(12), 4268–4273. <https://doi.org/10.1073/pnas.0400773101>
- Harbo, J. R. (2000). Heating Adult Honey Bees to Remove *Varroa Jacobsoni*. *Journal of Apicultural Research*, 39(3–4), 181–182. <https://doi.org/10.1080/00218839.2000.11101041>
- Howard, D., Duran, O., & Hunter, G. (2018). A Low-Cost Multi-Modal Sensor Network for the Monitoring of Honeybee Colonies/Hives. *Ambient Intelligence and Smart Environments*, 69–78. <https://doi.org/10.3233/978-1-61499-874-7-69>
- Human, H., Nicolson, S. W., & Dietemann, V. (2006). Do honeybees, *Apis mellifera* scutellata, regulate humidity in their nest? *Naturwissenschaften*, 93(8), 397–401.
- Humphrey, J. A. C., & Dykes, E. S. (2008). Thermal energy conduction in a honey bee comb due to cell-heating bees. *Journal of Theoretical Biology*, 250(1), 194–208. <https://doi.org/10.1016/j.jtbi.2007.09.026>
- Jones, J. C., Helliwell, P., Beekman, M., Maleszka, R., & Oldroyd, B. P. (2005). The effects of rearing temperature on developmental stability and learning and memory in the honey bee, *Apis mellifera*. *Journal of Comparative Physiology A*, 191(12), 1121–1129. <https://doi.org/10.1007/s00359-005-0035-z>

- Klein, B. A., Stiegler, M., Klein, A., & Tautz, J. (2014). Mapping Sleeping Bees within Their Nest: Spatial and Temporal Analysis of Worker Honey Bee Sleep. *PLOS ONE*, 9(7), e102316. <https://doi.org/10.1371/journal.pone.0102316>
- Kleinhenz, M. (2003). Hot bees in empty broodnest cells: Heating from within. *Journal of Experimental Biology*, 206(23), 4217–4231. <https://doi.org/10.1242/jeb.00680>
- Kronenberg, F., & Heller, H. C. (1982). Colonial thermoregulation in honey bees (*Apis mellifera*). *Journal of Comparative Physiology*, 148(1), 65–76. <https://doi.org/10.1007/BF00688889>
- Lecocq, A., Kryger, P., Vejsnæs, F., & Bruun Jensen, A. (2015). Weight Watching and the Effect of Landscape on Honeybee Colony Productivity: Investigating the Value of Colony Weight Monitoring for the Beekeeping Industry. *PLOS ONE*, 10(7), e0132473. <https://doi.org/10.1371/journal.pone.0132473>
- Lima, M. V., De Queiroz, J. P. A. F., Pascoal, L. A. F., Saraiva, E. P., Soares, K. O., & Evangelista-Rodrigues, A. (2019). Smartphone-based sound level meter application for monitoring thermal comfort of honeybees *Apis mellifera* L. *Biological Rhythm Research*, 1–14. <https://doi.org/10.1080/09291016.2019.1616144>
- Linear Technology. (2020). *Thermal resistance table* (p. 1). Analog Devices. <https://www.analog.com/media/en/package-pcb-resources/package/thermal-table.pdf>
- Meikle, W. G., Weiss, M., Maes, P. W., Fitz, W., Snyder, L. A., Sheehan, T., Mott, B. M., & Anderson, K. E. (2017). Internal hive temperature as a means of monitoring honey bee colony health in a migratory beekeeping operation before and during winter. *Apidologie*, 48(5), 666–680. <https://doi.org/10.1007/s13592-017-0512-8>
- Meikle, W., & Holst, N. (2015). Application of continuous monitoring of honeybee colonies. *Apidologie*, 46(1), 10–22. <https://doi.org/10.1007/s13592-014-0298-x>
- Meitalovs, J., Histjajevs, A., & Stalidz, E. (2009). Automatic microclimate controlled beehive observation system. *ENGINEERING FOR RURAL DEVELOPMENT*, 8, 265–271.
- Mezquida, D. A., & Martínez, J. L. (2009). Short communication.: Platform for bee-hives monitoring based on sound analysis. A perpetual warehouse for swarm's daily activity. *Spanish Journal of Agricultural Research*, 4, 824–828.
- Mills, R., Zahadat, P., Silva, F., Mlikic, D., Mariano, P., Schmickl, T., & Correia, L. (2015). Coordination of collective behaviours in spatially separated agents. *Artificial Life Conference Proceedings*, 27, 579–586. <https://doi.org/10.1162/978-0-262-33027-5-ch101>
- Nicolson, S. W. (2009). Water homeostasis in bees, with the emphasis on sociality. *Journal of Experimental Biology*, 212(3), 429–434. <https://doi.org/10.1242/jeb.022343>

- Ohashi, M., Okada, R., Kimura, T., & Ikeno, H. (2009). Observation system for the control of the hive environment by the honeybee (*Apis mellifera*). *Behavior Research Methods*, 41(3), 782–786. <https://doi.org/10.3758/BRM.41.3.782>
- Simone-Finstrom, M., Foo, B., Tarpy, D. R., & Starks, P. T. (2014). Impact of Food Availability, Pathogen Exposure, and Genetic Diversity on Thermoregulation in Honey Bees (*Apis mellifera*). *Journal of Insect Behavior*, 27(4), 527–539. <https://doi.org/10.1007/s10905-014-9447-3>
- Southwick, E. E., & Moritz, R. F. A. (1987). Social control of air ventilation in colonies of honey bees, *Apis mellifera*. *Journal of Insect Physiology*, 33(9), 623–626. [https://doi.org/10.1016/0022-1910\(87\)90130-2](https://doi.org/10.1016/0022-1910(87)90130-2)
- Stabentheiner, A., Kovac, H., & Brodschneider, R. (2010). Honeybee Colony Thermoregulation – Regulatory Mechanisms and Contribution of Individuals in Dependence on Age, Location and Thermal Stress. *PLoS ONE*, 5(1), e8967. <https://doi.org/10.1371/journal.pone.0008967>
- Stalidzans, E., Zacepins, A., Kviesis, A., Brusbardis, V., Meitalovs, J., Paura, L., Bulipopa, N., & Liepniece, M. (2017). Dynamics of Weight Change and Temperature of *Apis mellifera* (Hymenoptera: Apidae) Colonies in a Wintering Building With Controlled Temperature. *Journal of Economic Entomology*, 110(1), 13–23. <https://doi.org/10.1093/jee/tow282>
- Stefanec, M., Szopek, M., Schmickl, T., & Mills, R. (2017). Governing the swarm: Controlling a bio-hybrid society of bees robots with computational feedback loops. *2017 IEEE Symposium Series on Computational Intelligence (SSCI)*, 1–8. <https://doi.org/10.1109/SSCI.2017.8285346>
- Szopek, M., Schmickl, T., Thenius, R., Radspieler, G., & Crailsheim, K. (2013). Dynamics of Collective Decision Making of Honeybees in Complex Temperature Fields. *PLOS ONE*, 8(10), e76250. <https://doi.org/10.1371/journal.pone.0076250>
- Tautz, J., Maier, S., Groh, C., Rössler, W., & Brockmann, A. (2003). Behavioral performance in adult honey bees is influenced by the temperature experienced during their pupal development. *Proceedings of the National Academy of Sciences*, 100(12), 7343–7347. <https://doi.org/10.1073/pnas.1232346100>
- Vollet-Neto, A., Menezes, C., & Imperatriz-Fonseca, V. L. (2011). Brood production increases when artificial heating is provided to colonies of stingless bees. *Journal of Apicultural Research*, 50(3), 242–247. <https://doi.org/10.3896/IBRA.1.50.3.09>
- Zacepins, A., Brusbardis, V., Meitalovs, J., & Stalidzans, E. (2015). Challenges in the development of Precision Beekeeping. *Biosystems Engineering*, 130, 60–71.

<https://doi.org/10.1016/j.biosystemseng.2014.12.001>

Zhu, X., Wen, X., Zhou, S., Xu, X., Zhou, L., & Zhou, B. (2019). The temperature increase at one position in the colony can predict honey bee swarming (*Apis cerana*). *Journal of Apicultural Research*, 58(4), 489–491.

<https://doi.org/10.1080/00218839.2019.1632149>

Appendix A: Brood nest sensor array density model

Introduction

The primary concept here is to examine the density of sensing as a function of utility (defined below). We do not know *a priori* how many sensors will provide valuable information, since there are not many studies that examine the brood nest with multiple point measurements, and those that exist do not formally establish their choices. We therefore develop a simple model of a temperature field within a brood nest frame to evaluate the quality of different numbers of sensors in a grid.

Zhu et al (2019) develop panels comprising 36 digital temperature sensors, and motivate their investigation by the application (predicting swarming). Szabo (1985) inserted 9 thermistors into each of 6 combs, with a spacing of 7x7 cm, to measure the temperatures inside wintering hives in Canada. The factors driving the choice of 36 or 9 per panel with Langstroth-form dimensions are not stated. Becher & Moritz (2009) uses one sensor on the corner where each three cells meet, and thus 256 sensors estimate temperature of 768 cells. Their choice of 256 sensors is presumably due to pragmatic limits of address space and cost/effort, thus yielding a coverage that is bounded by the sensor count. However, the usage described in Becher et al (2010) is that 15x15 cm areas of brood were cut out from full combs and placed on the device to obtain data.

Since our instrument will remain in place throughout the season and we cannot know which area of any given comb the brood nest will occupy, we aim for broad coverage of the frame and here examine the tradeoff between sensing quality and sensor quantity.

The cells in brood areas of a beehive have several uses, including: brood, honey, nectar, empty (Camazine, 1991; Montovan et al., 2013). The temperature of the brood cells is tightly regulated by nurse bees (Bujok et al., 2002; Stabentheiner & Haggmüller, 1991), but for the other cell uses the regulation is not so strong. Moreover, there exist differences between the centre of the brood and the exterior or the brood (Dunham, 1931; Klein et al., 2014). The study of Becher et al (2010) presents temperatures measured in a 15x15 cm area of brood, and establishes a two-segment linear model: constant inside the core of the brood nest, and linear decrease to the edge of the sensed area (note that the decrease starts *inside* the brood nest, see fig A.1 a).

Model

We extend the two-segment linear model (Fig A.1 a) into a three-segment model. The original model has a uniform temperature T_B in the centre of the brood nest, and a linear decrease with distance from the brood centre. The third segment provides a lower limit temperature T_U far from the brood nest centre, where the cells are unoccupied. We model the brood nest as circular with radius r_b , the dropping segment to start at $r_c = r_b - r_r$ and stop at r_u (Fig A.1 b).

$$T(r) = \begin{cases} T_B, & \text{if } r < r_c, \\ \frac{r - (r_u - r_c)(T_B - T_U)}{r_u - r_c}, & \text{if } r_c < r < r_u, \\ T_U & \text{if } r > r_u \end{cases}$$

The size of the brood nest r_b is a variable. Following the data shown in Becher et al (2010) we define the ring radius $r_r = 2$ cm, and the slope as $dT/dr = 0.45$ °C / 1cm which thus yields the dimension r_u . The brood nest core temperature, $T_B=34.5$ °C, is taken from Becher et al (2010), and the temperature of the unoccupied region is defined as $T_U=25.0$ °C.

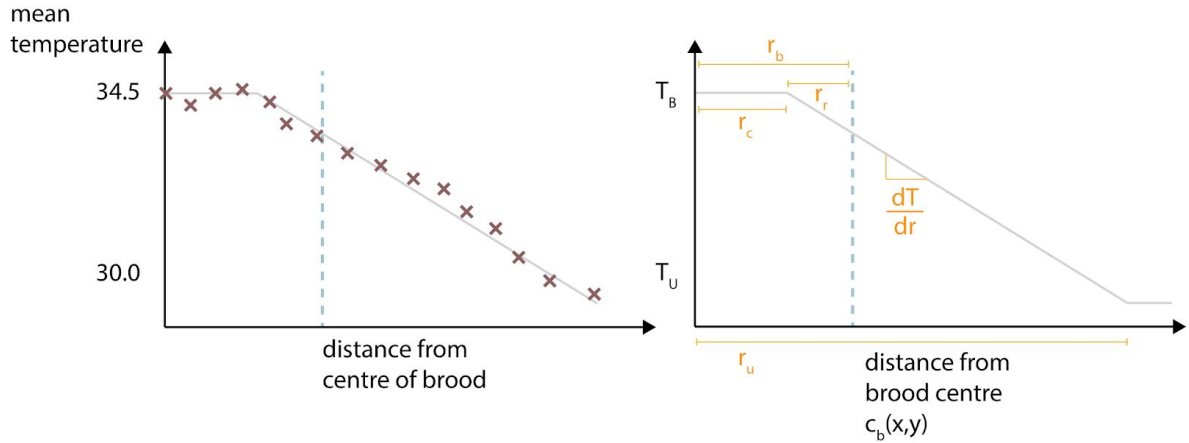


Fig A.1: brood nest temperature profile. a) data and approximation, following fig 1 of Becher et al (2010). b) generalised three-segment model, with parameters as described in the text. The dashed vertical lines indicate the edge of the brood nest.

For a given quantity of simulated sensors, we define their location to be on a regular grid to fill a Zander frame of 42x20 cm.

Quantification metric:

For a given parameter combination $(c_b(x,y), r_b, h, w)$, corresponding to brood nest centre position (c_b), radius (r_b), the number of sensors oriented vertically (h) and horizontally (w), we compute the error (ϵ) as follows.

The sensors make “point samples” at their location (x,y) in their temperature field. All other locations are estimated by linear interpolation between the nearest sensors in the mesh, $\hat{T}(x,y)$. We thus arrive at two matrices, the simulated temperature field across the frame, T , and the estimates, \hat{T} . The error is defined as

$$\epsilon(c_b(x,y), r_b, h, w) = \frac{1}{h \cdot w} \sum_x \sum_y |T - \hat{T}|.$$

Our objective is to select the number of sensors (h, w) and so we take the mean error ϵ over all combinations of $(c_b(x,y), r_b)$ as the metric $E(h, w)$.

Fig. A.2 provides an illustration of the model and example simulated sensor points.

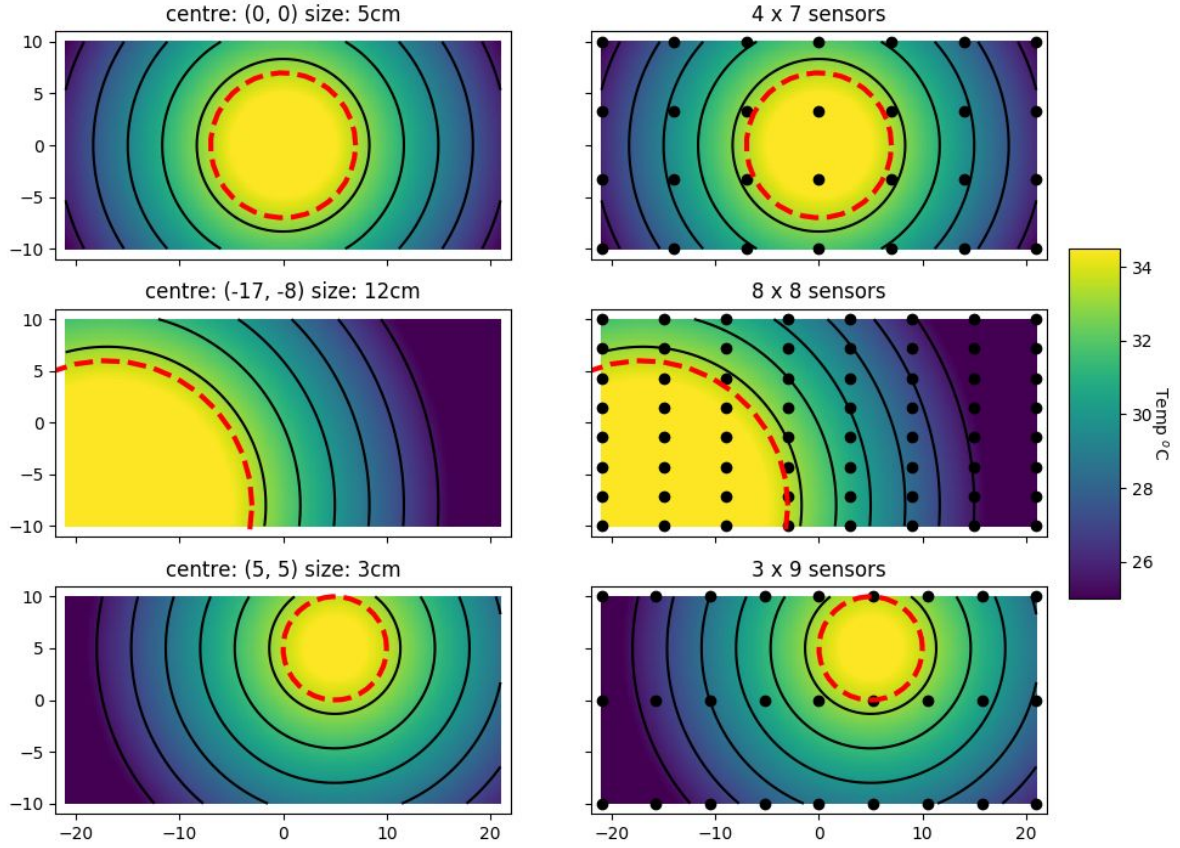


Fig A.2: Example parameter combinations used in the temperature field model. The red dashed line indicates the limit of the brood nest. The left column illustrates modelled brood nest locations and their radii; the right column illustrates three different combinations of sensor arrays.

Simulation results and discussion

A summary of the model results are shown in Fig A.3, comprising approximately 44000 samples. The vertical dashed lines indicate banks of 32 sensors, which are limits per I2C channel (described further below). It is clear that exceeding a single bank of 32 is clearly advantageous, but exceeding 64 sensors the incremental benefit of further sensors drops substantially. In any case, we achieve sub-0.1 °C mean error for all configurations with greater than 3 rows.

The geometry has an impact that is only partially revealed by the scalar metric E , for example, a single row of 64 sensors has large errors in estimation far from that row and is clearly a poor choice. Generally a large imbalance between x- and y- spacing should be avoided, since we have no strong priors to support considering horizontal data being significantly less or more valuable than vertical information.

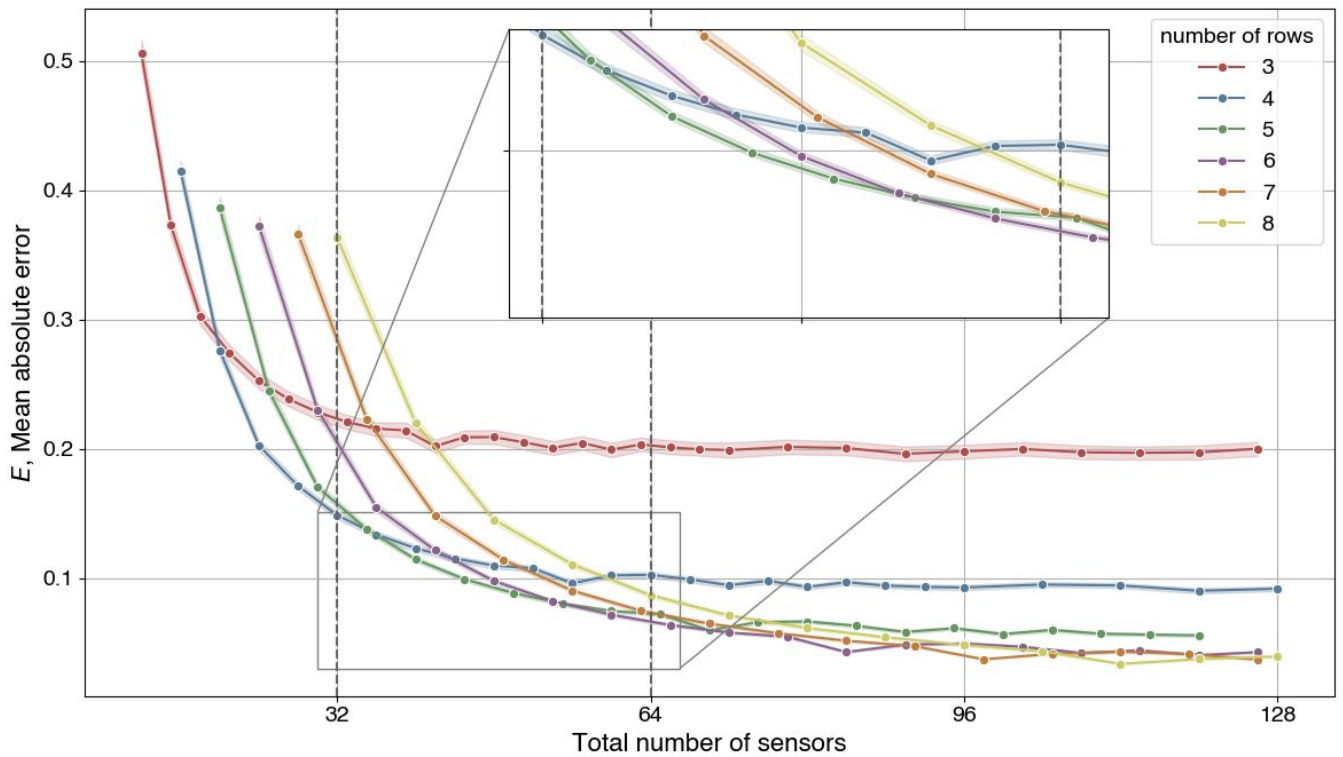


Fig A.3: Mean error quantification for various sensor quantities. Vertical dashed lines at 32 or 64 elements (32 devices connectable per I2C channel). Inset shows detail for the region where our selection should be made.

The general trend clearly shows that there are diminishing returns with increasing sensor density, and that sub-0.1 °C mean error is achievable with 64 or fewer sensors.

Engineering limits

The choice of sensor, the TMP117, was made based on performance requirements (see D5.1, sec 3.1.1). It communicates via an I2C bus, and has four different addresses (selected by wiring address pins to Vcc or Gnd). Using 8-way multiplexers we can address 32 sensors per I2C channel.

Horizontal and vertical spacing

Tables A.1 and A.2 show candidate spacing for our target Zander frame dimensions (410 x 180 mm area that the bees can access within the whole frame of 420 x 210 mm). Based on the objectives outlined, 11 x 5 or 15 x 6 sensors fit within 2 channels (64 devices) or 3 (96 devices). The improvement in E obtained by using 15 x 6 sensors is only approximately 0.03 °C and the additional cost and increase in complexity to supporting this many sensors is not justified. Conversely, moving past 32 sensors is required to measure at an error of lower than 0.15 °C. The trade-off of cost per brood board and sensed resolution, for this V2 prototype was settled to be 5 rows x 11 columns.

H	H spacing		V	V spacing
7	55.7 mm		4	40.0 mm
9	43.3 mm		5	32.0 mm
11	35.5 mm		6	26.7 mm
13	30.0 mm		7	22.9 mm
15	26.0 mm		8	20.0 mm
17	22.9 mm			

Table A.1: Number of rows and columns and their approximate spacing within a Zander frame, assuming 10mm border before the first sensor is placed.

H	V	Mm x mm	HxV=n
9	4	43x40	36
11	5	35x32	55
15	6	26x26	90
17	7	23x20	119

Table A.2: Candidates for balanced horizontal and vertical spacing

Geometric considerations

We have two primary geometric considerations: 1) we generally prefer to define an evenly-spaced mesh in each dimension; and 2) the mechanical design of the module includes a foundation layer to guide the cell formation, and accordingly the precise locations for sensors should be constrained by the cell locations.

Finally, the controllers for the 10 heater elements (see D5.1, Sec 3) require at least one sensor on each patch. While this requirement is likely to be met by any of the choices, it must be verified.

Fig A.4 shows the precise dimensions for the foundation layer hexagons. We use integer multiples of the rows and columns to align the sensors with these hexagons. Note that for cells to be vertically aligned we jump over two rows, meaning the vertical centre-centre spacing is 9.1 mm.

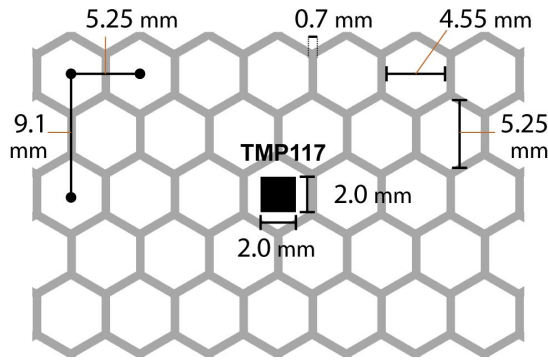


Fig A.4: Hexagon dimensions and alignment of target distances

To obtain an approximate 32 mm vertical interval, we select 4 steps (36.4 mm). To obtain the approximate horizontal interval of 35 mm, we select 7 steps (36.75 mm). The final layout for the sensors is shown in fig A.5.

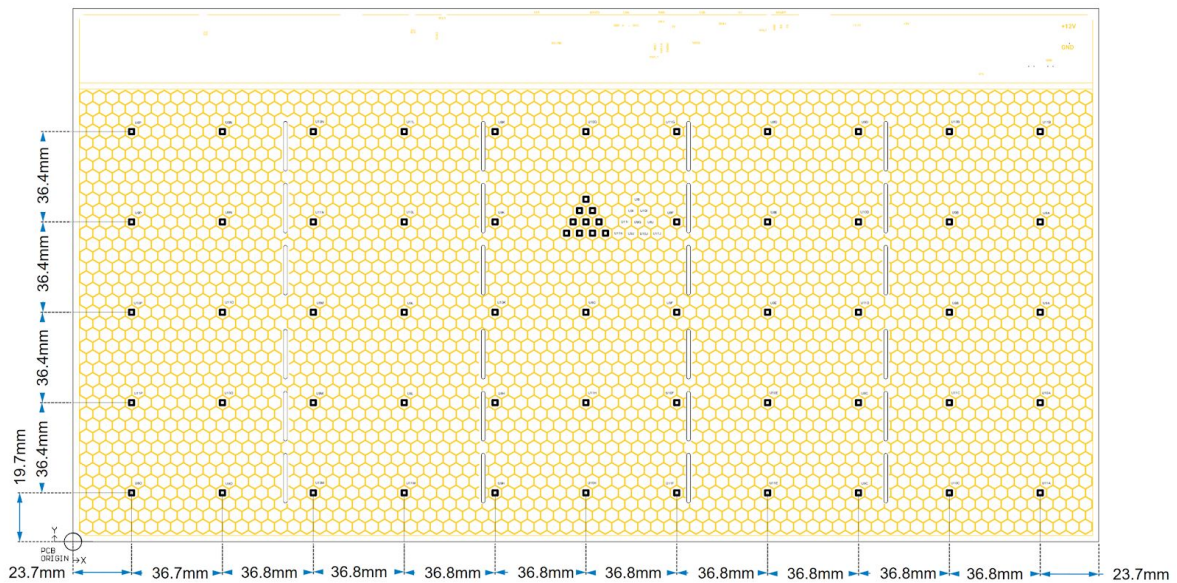


Fig A.5: Final placement, showing sensors, hexagons, and heater regions

Various aspects of this modelling study could benefit from elaboration. The brood nest is always modelled as a single circular patch; this could be generalised, e.g. to multiple elliptical forms. The piecewise linear model is a simplification, and could be substituted by detailed brood thermal models (e.g. Humphrey & Dykes, 2008) or our measured data (see D5.1, sec 2.3). Overall, the loss-function here is defined at a low level but we also envisage developing a higher-level loss function that is more task-oriented, e.g., the ability to localise brood nest patches of a certain area. A somewhat different direction for exploration is subset selection of a sensor array, and/or non-uniform placements. These have been examined in various applications (e.g. (Husain, 1989; Krause et al., 2006; Lee et al., 2014; Staszewski & Worden, 2001)) but we do not at present have data from a sufficient number of experimental runs (i.e., with enough diversity to cover most likely brood spatial and temperature patterns).

Nonetheless, the present model was sufficient to explore the relative differences in sensing errors for different sensor quantities and aid our design process. Our choice that balances

the sensing quality and cost per board is to use 55 sensors, in 5 rows each with 11 sensors. This results in sensors being fairly close to equally spaced in x- and y- dimension, and also fits the geometry of a hexagon mesh. The predicted mean absolute error is under 0.1°C, which is within the resolution of the sensor. This density of sensing should allow us to localise the brood nest and use its temporal temperature signature as health-state indicators.

References cited in appendix

- Becher, M. A., Hildenbrandt, H., Hemelrijk, C. K., & Moritz, R. F. A. (2010). Brood temperature, task division and colony survival in honeybees: A model. *Ecological Modelling*, 221(5), 769–776. <https://doi.org/10.1016/j.ecolmodel.2009.11.016>
- Becher, M. A., & Moritz, R. F. A. (2009). A new device for continuous temperature measurement in brood cells of honeybees (*Apis mellifera*). *Apidologie*, 40(5), 577–584. <https://doi.org/10.1051/apido/2009031>
- Bujok, B., Kleinhenz, M., Fuchs, S., & Tautz, J. (2002). Hot spots in the bee hive. *Naturwissenschaften*, 89(7), 299–301. <https://doi.org/10.1007/s00114-002-0338-7>
- Camazine, S. (1991). Self-organizing pattern formation on the combs of honey bee colonies. *Behavioral Ecology and Sociobiology*, 28(1), 61–76. <https://doi.org/10.1007/BF00172140>
- Dunham, W. E. (1931). Hive Temperatures for Each Hour of a Day. *The Ohio Journal of Science*, 31(3), 181–188.
- Humphrey, J. A. C., & Dykes, E. S. (2008). Thermal energy conduction in a honey bee comb due to cell-heating bees. *Journal of Theoretical Biology*, 250(1), 194–208. <https://doi.org/10.1016/j.jtbi.2007.09.026>
- Husain, T. (1989). Hydrologic uncertainty measure and network design. *JAWRA Journal of the American Water Resources Association*, 25(3), 527–534. <https://doi.org/10.1111/j.1752-1688.1989.tb03088.x>
- Klein, B. A., Stiegler, M., Klein, A., & Tautz, J. (2014). Mapping Sleeping Bees within Their Nest: Spatial and Temporal Analysis of Worker Honey Bee Sleep. *PLOS ONE*, 9(7), e102316. <https://doi.org/10.1371/journal.pone.0102316>

- Krause, A., Guestrin, C., Gupta, A., & Kleinberg, J. (2006). Near-optimal sensor placements: Maximizing information while minimizing communication cost. *Proceedings of the 5th International Conference on Information Processing in Sensor Networks*, 2–10.
<https://doi.org/10.1145/1127777.1127782>
- Lee, C., Paik, K., & Lee, Y. (2014). Optimal sampling network for monitoring the representative water quality of an entire reservoir on the basis of information theory. *Journal of Water and Climate Change*, 5(2), 151–162.
<https://doi.org/10.2166/wcc.2014.104>
- Montovan, K. J., Karst, N., Jones, L. E., & Seeley, T. D. (2013). Local behavioral rules sustain the cell allocation pattern in the combs of honey bee colonies (*Apis mellifera*). *Journal of Theoretical Biology*, 336, 75–86. <https://doi.org/10.1016/j.jtbi.2013.07.010>
- Stabentheiner, A., & Hagmüller, K. (1991). Sweet food means “Hot Dancing” in honeybees. *Naturwissenschaften*, 78(10), 471–473. <https://doi.org/10.1007/BF01134389>
- Staszewski, W. J., & Worden, K. (2001). *Overview of optimal sensor location methods for damage detection* (V. S. Rao, Ed.; pp. 179–187). <https://doi.org/10.1117/12.436472>
- Szabo, T. I. (1985). The Thermology of Wintering Honeybee Colonies in 4-Colony Packs as Affected by Various Hive Entrances. *Journal of Apicultural Research*, 24(1), 27–37.
<https://doi.org/10.1080/00218839.1985.11100645>
- Zhu, X., Wen, X., Zhou, S., Xu, X., Zhou, L., & Zhou, B. (2019). The temperature increase at one position in the colony can predict honey bee swarming (*Apis cerana*). *Journal of Apicultural Research*, 58(4), 489–491.
<https://doi.org/10.1080/00218839.2019.1632149>

Appendix B: Brood nest components and libraries

Prototype v1 brood nest system

For reference, we maintain a list of hardware components and software libraries used in the system.

Component	model	quantity	note
Microcontroller board	Arduino MEGA 2560	1	https://store.arduino.cc/arduino-mega-2560-rev3
Temperature sensor	Dallas DS18B20+	88	https://datasheets.maximintegrated.com/en/ds/DS18B20.pdf
CO2 sensor	Sensirion SCD-30	1	https://developer.sensirion.com/fileadmin/user_upload/customers/sensirion/Dokumente/9.5_CO2/Sensirion_CO2_Sensors_SCD30_Datasheet.pdf https://www.sensirion.com/en/environmental-sensors/carbon-dioxide-sensors/carbon-dioxide-sensors-co2/
Camera	Raspberry Pi NoIR camera V2	2	https://www.raspberrypi.org/products/pi-noir-camera-v2/
Single-board computer for camera	Raspberry Pi model 3B	2	https://www.raspberrypi.org/products/raspberry-pi-3-model-b-plus

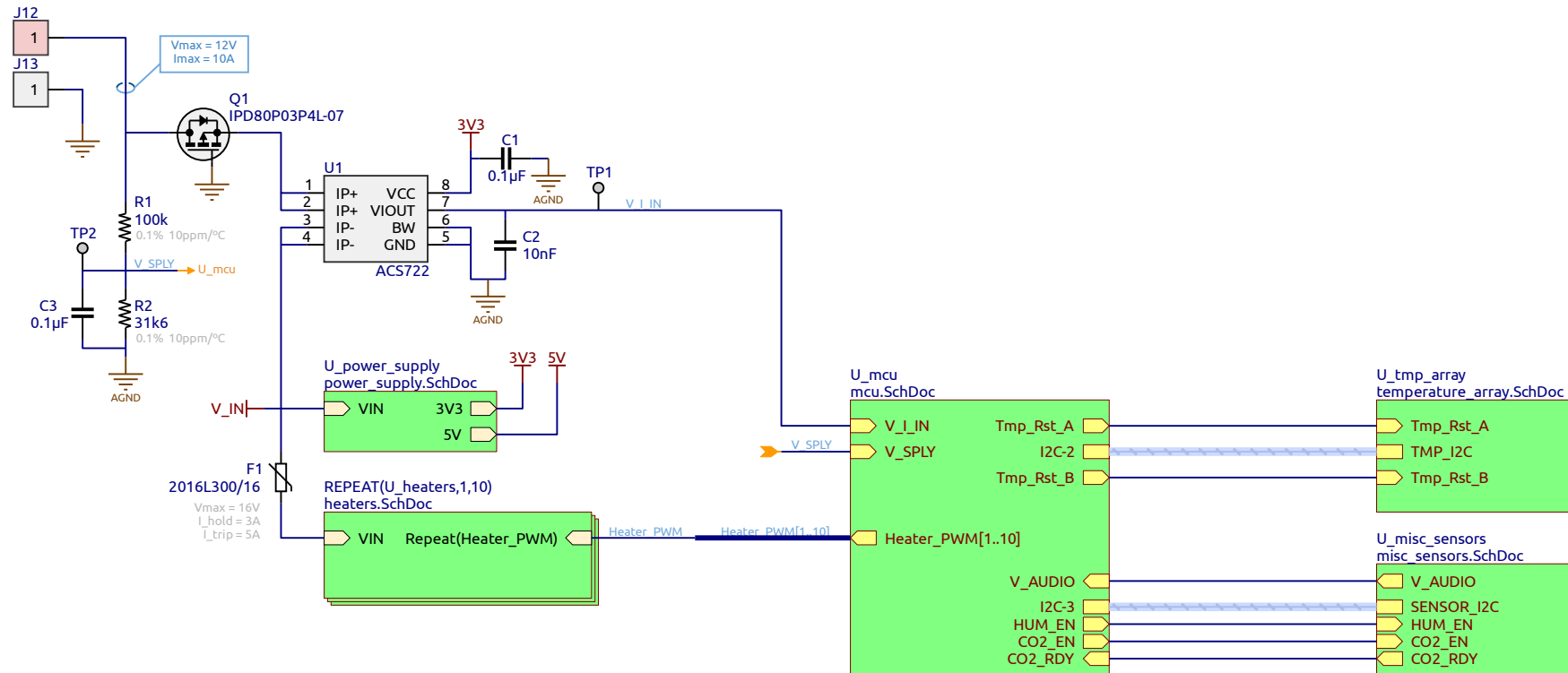
Purpose	Library	version
Operating system on camera single-board computer	Raspbian Buster Lite	Kernel 4.19
Camera SBC scripts	Python	3.6
Camera SBC scripts	Picamera library	1.13
Camera SBC scripts	systemd	241
Camera SBC scripts	OpenCV 3.4, with python bindings	3.4
Background subtraction	OpenCV::BackgroundSubtractorMOG2	3.4.9

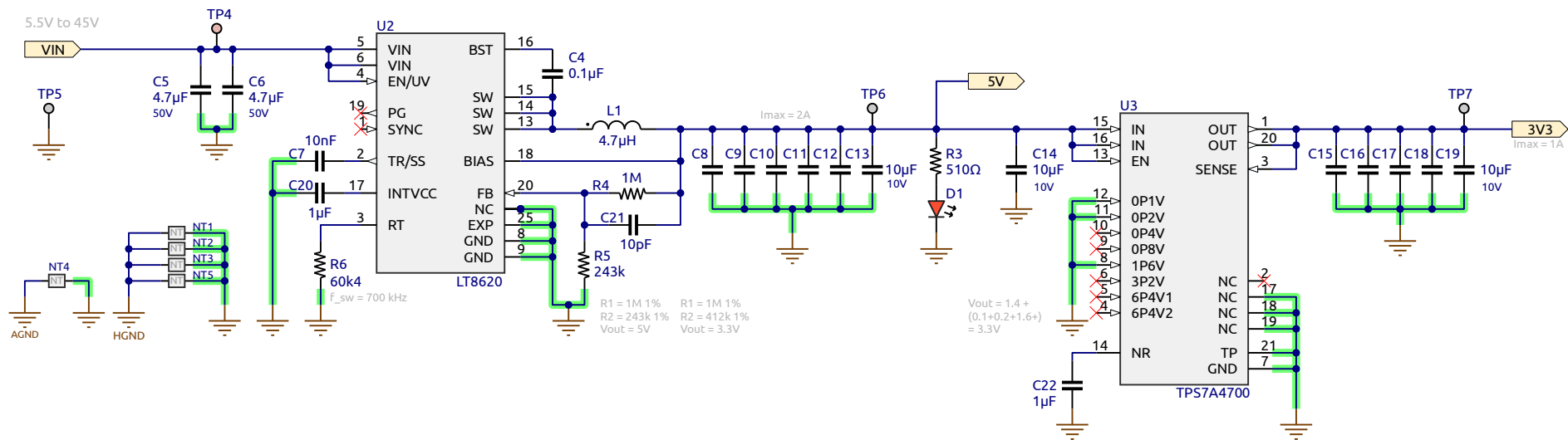
All software used has open-source licensing.

Prototype v2 brood nest system

For reference, we maintain a list of hardware components and software libraries used in the revised system.

Component	model	quantity	note
Candidate temperature sensor	Maxim MAX30205	0	Rejected at final round. https://www.maximintegrated.com/en/products/interface/sensor-interface/MAX30205.html
Temperature sensor	Texas TMP117	55 per brood frame (main array)	https://www.ti.com/product/TMP117
CO2 sensor	Sensirion SCD-30	1 per brood frame	https://www.sensirion.com/en/environmental-sensors/carbon-dioxide-sensors/carbon-dioxide-sensors-co2/
Camera	Raspberry Pi NoIR camera V2	2 per frame	https://www.raspberrypi.org/products/pi-noir-camera-v2/
Single-board computer for camera	Raspberry Pi model 3B	2 per frame	https://www.raspberrypi.org/products/raspberry-pi-3-model-b





Project **Brood Nest Sensing PCB**

Part **Power Supply**

Notes

File: **power_supply.SchDoc**

Date: 23-Mar-20

WP 5

Revision: **A**

Page 2 of 8

Authors:

Rafael Barmak*

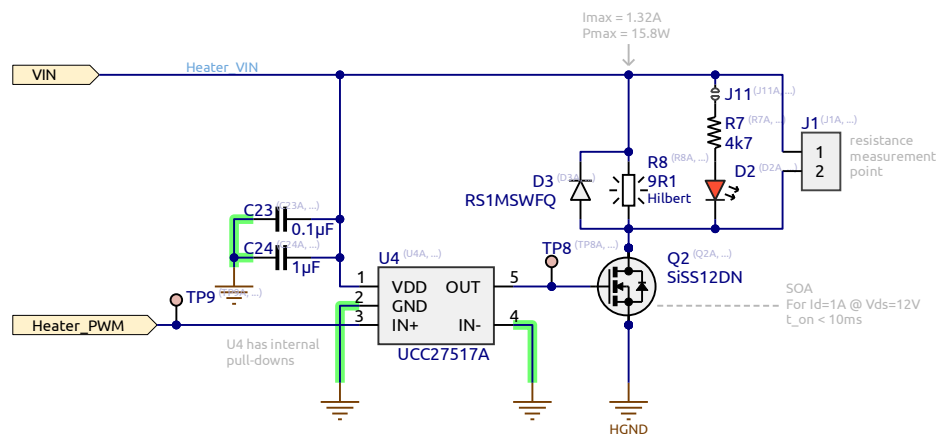
Rob Mills

Daniel Burnier

Eliot Ferragni



EPFL
MOBOTS / BIOROB
ME.B3.30, Station 9
Lausanne, 1015



Project **Brood Nest Sensing PCB**

Part **Heaters**

Notes

File: heaters.SchDoc

Date: 23-Mar-20

WP 5

Revision: **A**

Page 3 of 8

Authors:

Rafael Barmak*

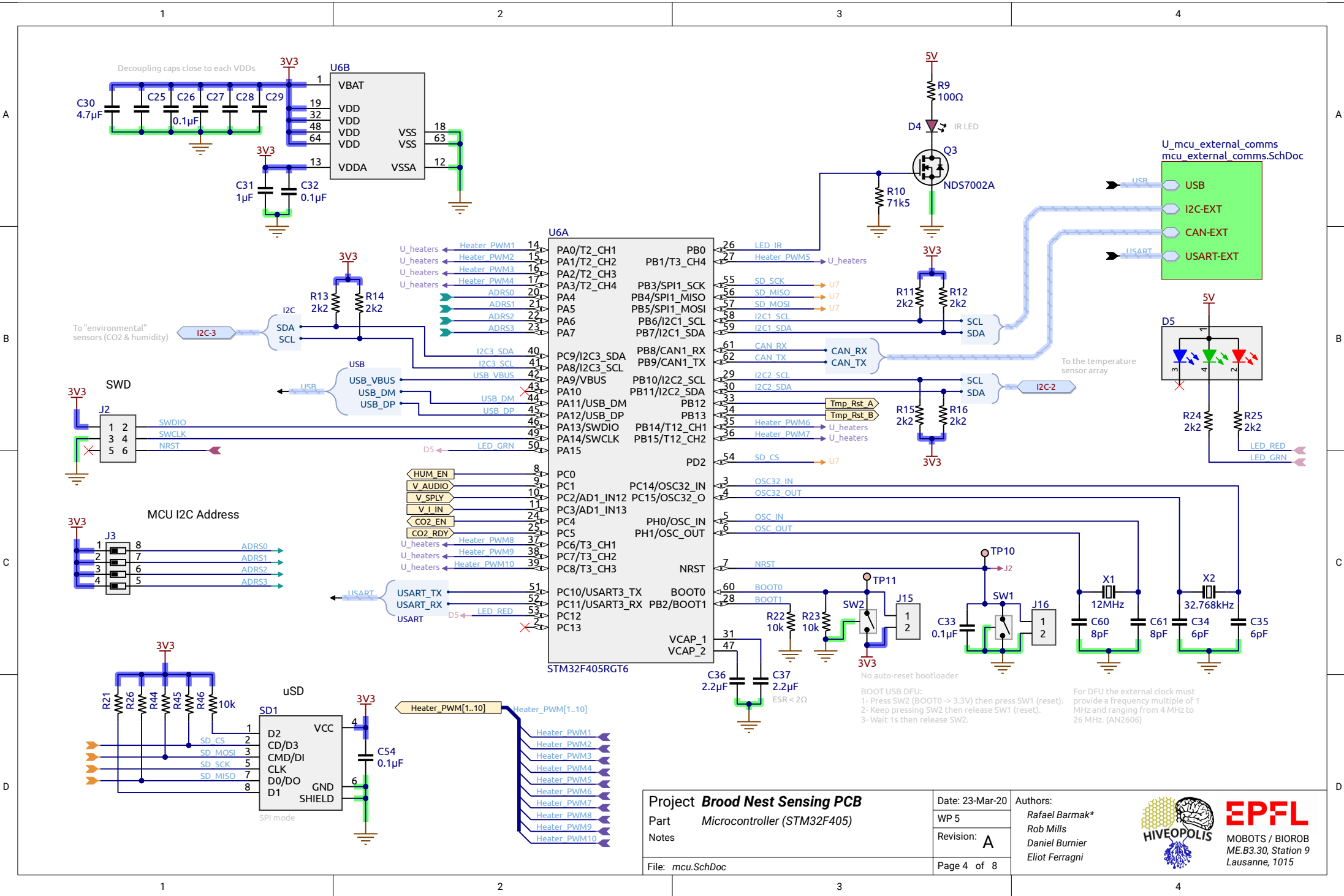
Rob Mills

Daniel Burnier

Eliot Ferragni



EPFL
MOBOTS / BIOROB
ME.B3.30, Station 9
Lausanne, 1015



Project **Brood Nest Sensing PCB**

Part **Microcontroller (STM32F405)**

Notes

File: **mcu.SchDoc**

Date: 23-Mar-20

WP 5

Revision: **A**

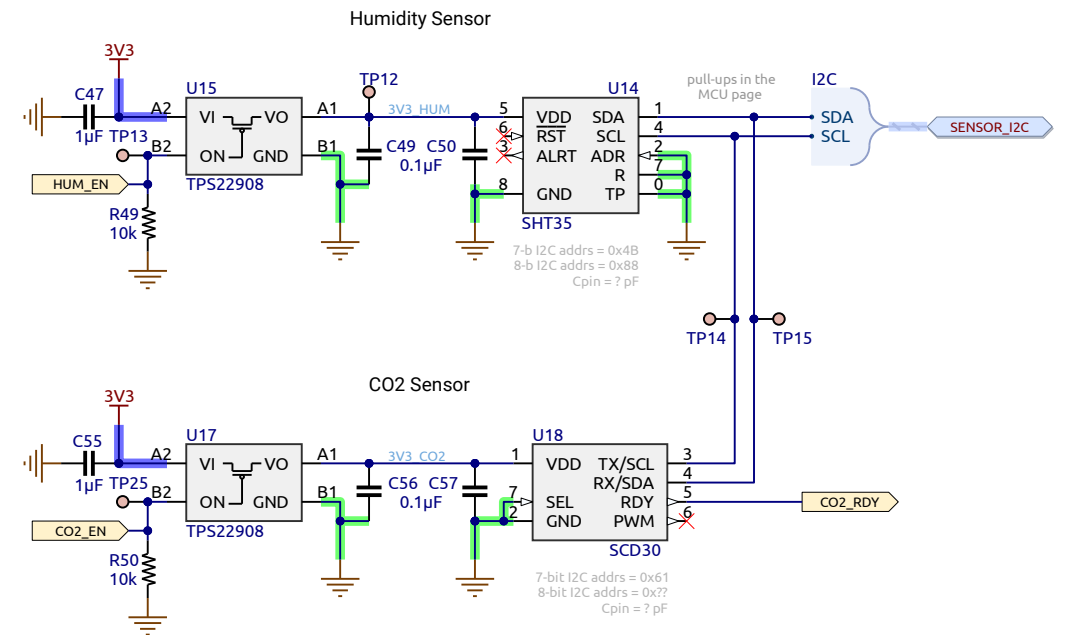
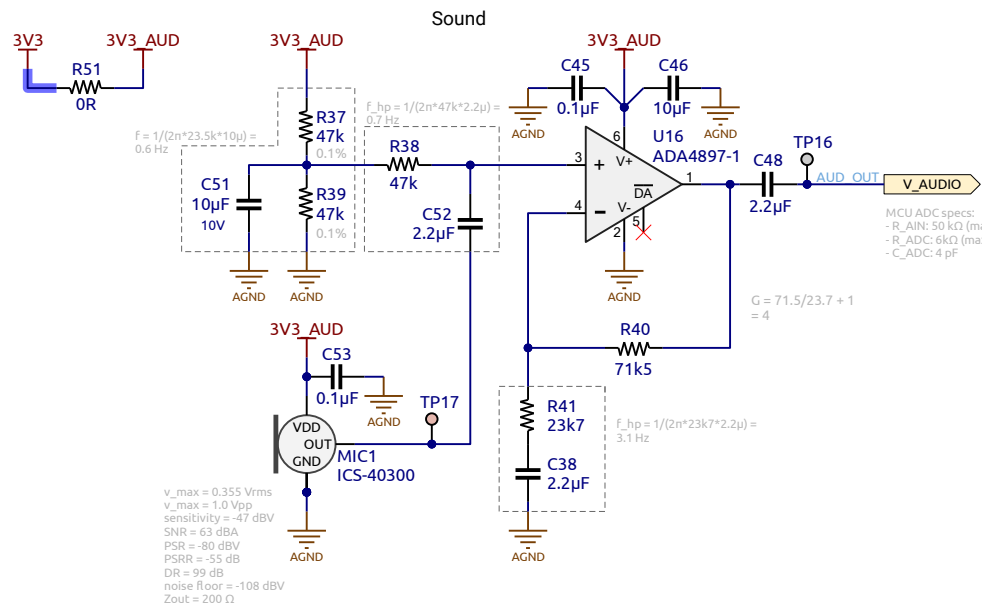
Page 4 of 8



Authors:

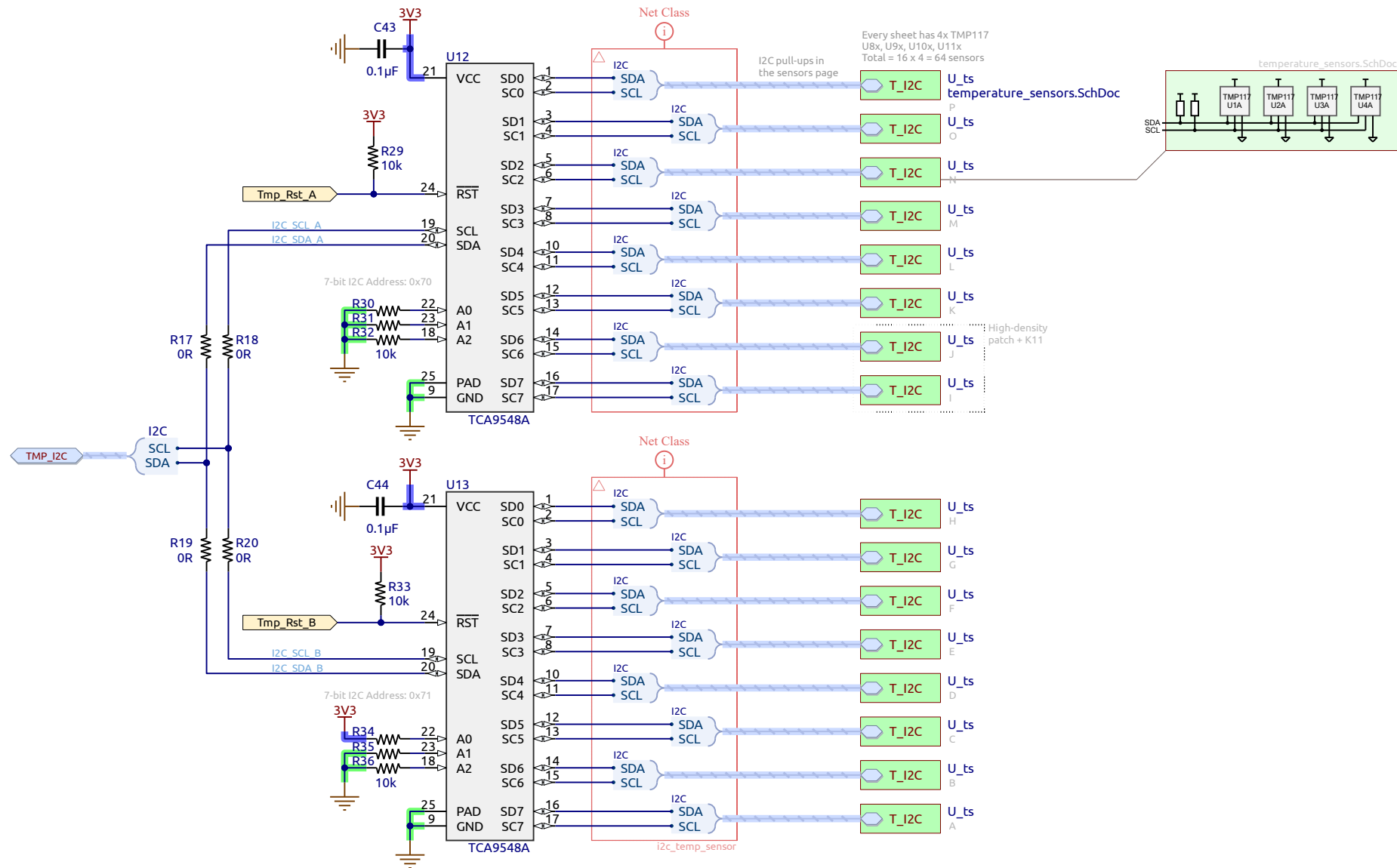
Rafael Barmak*
Rob Mills
Daniel Burnier
Eliot Ferragni



EPFL
MOBOTS / BIOROB
ME.B3.30, Station 9
Lausanne, 1015



Project Brood Nest Sensing PCB	Date: 23-Mar-20	Authors: Rafael Barmak* Rob Mills Daniel Burnier Eliot Ferragni	 
	Part Misc. sensors		
	Notes		
	File: misc_sensors.SchDoc		
	WP 5	Revision: A	MOBOTs / BIOROB ME.B3.30, Station 9 Lausanne, 1015
		Page 6 of 8	



Project **Brood Nest Sensing PCB**

Part **Temperature array**

Notes

File: *temperature_array.SchDoc*

Date: 23-Mar-20

WP 5

Revision: **A**

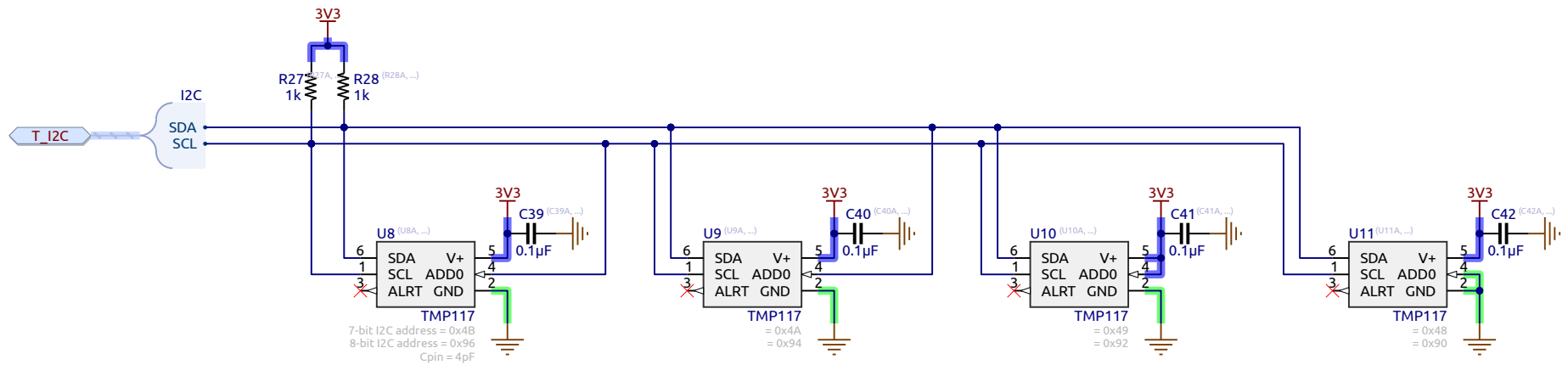
Page 7 of 8

Authors:

Rafael Barmak*
Rob Mills
Daniel Burnier
Eliot Ferragni



EPFL
MOBOTS / BIOROB
ME.B3.30, Station 9
Lausanne, 1015



Pull-up calculations:

Min Res for 3.3V:
 $R_{Pmin} = (VDD - V_{OLmax}) / I_{OL}$
 $R_{Pmin} = (3.3 - 0.4) / 3mA$
 $R_{Pmin} = 967 \Omega$

Max Bus Cap for R_{Pmin} :
 $tr = R_{Pmin} \times Cb$
 $Cb = tr / R_{Pmin} = 300ns / 967R$
 $Cb = 310 pF$

Max Res for $C_{bus} = 200pF$:
 $R_{Pmax} = tr / (0.8473 \times Cb)$
 $R_{Pmax} = 300ns / (0.847 \times 200pF)$
 $R_{Pmax} = 1.7 k\Omega$

Cb max for a $Rp = 2k2$:
 $Cb = tr / (0.8473 \times Rp)$
 $Cb = 300ns / (0.847 \times 2.2k)$
 $Cb = 160 pF$

<https://www.ti.com/lit/an/slva689/slva689.pdf>

Project **Brood Nest Sensing PCB**

Part **Temperature sensors**

Notes

File: **temperature_sensors.SchDoc**

Date: 23-Mar-20

WP 5

Revision: **A**

Page 8 of 8

Authors:

Rafael Barmak*
 Rob Mills
 Daniel Burnier
 Eliot Ferragni



EPFL
 ROBOTS / BIOROB
 ME.B3.30, Station 9
 Lausanne, 1015

Temperature sensors address map

29-Mar-2020

Multiplexers

- MUX U12: 0x70
- MUX U13: 0x71

High density patch

